Published April 18, 2011

Isoform-specific targeting of PKA to multivesicular bodies

Michele E. Day,[1,2] Guido M. Gaietta,[5] Mira Sastri,[3] Antonius Koller,[4] Mason R. Mackey,[5] John D. Scott,[6,7] Guy A. Perkins,[5] Mark H. Ellisman,[5] and Susan S. Taylor[2,3,4]

[1]Bioinformatics Program, [2]Department of Pharmacology, [3]Department of Chemistry and Biochemistry, [4]Howard Hughes Medical Institute, and [5]National Center for Microscopy and Imaging Research, University of California at San Diego, La Jolla, CA 92093
[6]Howard Hughes Medical Institute and [7]Department of Pharmacology, University of Washington School of Medicine, Seattle, WA 98195

Although RII protein kinase A (PKA) regulatory subunits are constitutively localized to discrete cellular compartments through binding to A-kinase–anchoring proteins (AKAPs), RI subunits are primarily diffuse in the cytoplasm. In this paper, we report a novel AKAP-dependent localization of RIα to distinct organelles, specifically, multivesicular bodies (MVBs). This localization depends on binding to AKAP11, which binds tightly to free RIα or RIα in complex with catalytic subunit (holoenzyme). However, recruitment to MVBs occurs only with the release of PKA catalytic subunit (PKAc). This recruitment is reversed by reassociation with PKAc, and it is disrupted by the presence of AKAP peptides, mutations in the RIα AKAP-binding site, or knockdown of AKAP11. Cyclic adenosine monophosphate binding not only unleashes active PKAc but also leads to the targeting of AKAP11:RIα to MVBs. Therefore, we show that the RIα holoenzyme is part of a signaling complex with AKAP11, in which AKAP11 may direct RIα functionality after disassociation from PKAc. This model defines a new paradigm for PKA signaling.

Introduction

Although PKA has been extensively studied for decades, the focus has mainly been on its catalytic subunit activity or the PKA holoenzyme (heterotetramers of regulatory and catalytic subunits). The role of its regulatory subunits (R-subunits) that is independent of the PKA catalytic subunits (PKAc's) has not been well characterized. The classically known functions of R-subunits are to inhibit PKAc and facilitate in targeting PKAc to compartmentalized regions of the cell by binding to A-kinase–anchoring proteins (AKAPs) at its N-terminal domain (dimerization/docking [D/D] domain). Through the binding of cAMP at the C-terminal domains of R-subunits, PKAc is released from the holoenzyme complex and activated to phosphorylate downstream substrates.

Two general classes of R-subunits exist, RI and RII (Reimann et al., 1971), which can be further resolved at the genetic level into four separate gene products: RIα, RIβ, RIIα, and RIIβ (Lee et al., 1983; Jahnsen et al., 1986; Scott et al., 1987; Clegg et al., 1988). Although over 50 AKAPs have been identified (Wong and Scott, 2004), the majority of them bind to RII subunits so that RII subunits are typically associated with membranous organelles. Meanwhile, because RI subunits are mainly diffused in the cytoplasm, the localization of the RI holoenzyme has received less attention and is not well appreciated. Several studies have indicated that RIα, probably associated with PKAc, can be recruited to specific sites, for example, to the "cap" site of activated T lymphocytes (Levy et al., 1996). The RI holoenzyme also localized to microtubules during the entire cell cycle (Imaizumi-Scherrer et al., 2001) and to protrusions at the front of migrating cells through its interaction with α4 integrin (Lim et al., 2007).

G.M. Gaietta and M. Sastri contributed equally to this paper.

Correspondence to Susan S. Taylor: staylor@ucsd.edu

A. Koller's present address is Proteomics Center, Stony Brook University Medical Center, Stony Brook, NY 11794.

Abbreviations used in this paper: AIF, apoptosis-inducing factor; AKAP, A-kinase–anchoring protein; AKB, A-kinase binding; AQP2, aquaporin 2; D/D, dimerization/docking; EEA1, early endosome antigen 1; HEK, human embryonic kidney; IBMX, isobutylmethylxanthine; IP, immunoprecipitation; LC3, light chain 3; MEF, mouse embryonic fibroblast; MVB, multivesicular body; PKAc, PKA catalytic subunit; PKI, protein kinase inhibitor; PMP70, 70-kD peroxisomal membrane protein; R-subunit, regulatory subunit; TAP, tandem affinity purification.

Supplemental Material can be found at:
http://jcb.rupress.org/content/suppl/2011/04/18/jcb.201010034.DC1.html

The Rockefeller University Press $30.00
J. Cell Biol. Vol. 193 No. 2 347–363
www.jcb.org/cgi/doi/10.1083/jcb.201010034

Published April 18, 2011

Although free RI was previously reported to be less stable when not in complex with PKAc (Steinberg and Agard, 1981; Orellana and McKnight, 1990), more recent studies have revealed that free RI subunits localize to subcellular sites beyond the cytoplasm. For example, some studies have shown the association of RI with membranes (Rubin, 1979; Boeshans et al., 1999). Another study reported that, independent of PKAc, the N terminus of RIα, but not RII, was needed to bind RFC40 and transport it into the nucleus (Gupte et al., 2005). In addition, this translocation from the cytoplasm to the nucleus has been correlated with the formation of the interchain disulfide bonds found in the D/D domain of RI but not found in RII (Brennan et al., 2006). Mavrakis et al. (2006) also reported the localization of RIα to late endosomes and autophagosomes.

Because the function of a protein is closely linked to its subcellular location, the different localizations of R-subunit isoforms could explain some of their known functional differences. RIα is the only isoform that acted as a tissue-specific extinguisher (Boshart et al., 1991; Jones et al., 1991) and the only one that has been pursued as an anticancer drug target (Chen et al., 2000; Goel et al., 2006). Its down-regulation or overexpression disrupted normal cell cycle progression (Tortora et al., 1994a,b). It was also the only isoform that resulted in embryonic lethality when deleted in mice (Amieux and McKnight, 2002). On the other hand, deletion of RIβ resulted in defects in hippocampal function (Brandon et al., 1995). Deletion of RIIα showed no gross organ dysfunction (Burton et al., 1999), whereas deletion of RIIβ resulted in several changes, such as a lean phenotype with elevated body temperatures and metabolic rates (McKnight et al., 1998) or a decreased sensitivity to increased ethanol consumption (Thiele et al., 2000). Thus, although four isoforms of the R-subunits exist, they are not functionally redundant.

RIα is also the only isoform that can compensate for excess PKAc activity. When PKAc was overexpressed in NIH 3T3 cells, RIα levels increased with no change in RII subunit levels (Uhler and McKnight, 1987). RIα knockout mice were no longer embryonically lethal when PKAc was also knocked out, but the double knockout mice displayed developmental defects later in life (Amieux and McKnight, 2002). Thus, a tightly coordinated regulation exists between RIα and PKAc that is crucial for normal development.

RIα may also have functions independent of PKAc. Overexpression of RIα is associated with breast cancer (Miller, 2002), whereas underexpression of RIα is linked to systemic lupus erythematosus (Kammer et al., 1996; Laxminarayana et al., 1999) and Carney complex (Kirschner et al., 2000). Mutations in RIα that did not affect RIα expression levels or PKAc activity still resulted in Carney complex (Veugelers et al., 2004). In light of these findings, the localization of RIα in the absence of PKAc is important to characterize.

In this study, we investigate a novel localization of RIα that was observed after expression in mammalian cells. In contrast to the other proteins we expressed, RIα formed puncta. The aims of our study were to characterize these puncta and determine their requirements for formation. By expressing RIα-GFP in HeLa and RIα knockout mouse embryonic fibroblasts (MEFs), we showed that these puncta were RI specific. Furthermore, we established that it was free RI subunit that was required for formation, as overexpressed RIα holoenzyme was cytoplasmic and showed no evidence of puncta formation. Upon stimulation with forskolin/isobutylmethylxanthine (IBMX), however, puncta formation occurred and was reversible for up to 3 h. Using fractionation and correlated light and electron microscopy, we established that RIα puncta localized to multivesicular bodies (MVBs). Through mutagenesis experiments or coexpression with isoform-specific AKAP-disrupting peptides, we demonstrated that AKAP binding was essential for this localization. In addition, our knockdown experiments established that it required a specific AKAP, AKAP11 (also known as AKAP220). Finally, we determined that the endogenous RIα holoenzyme, though diffuse in the cytoplasm, was still tightly associated with AKAP11; however, translocation to MVBs only occurred when PKAc was released. Therefore, in contrast to RII subunits, which appear constitutively localized to discrete regions of the cell via high affinity binding to AKAPs, RIα is assembled with AKAP11 as a soluble and cytoplasmic signaling complex. Then, upon stimulation with cAMP, AKAP11:RIα can be dynamically recruited to specific sites. We thus show that AKAP11 is highly specific for RIα and also define a new paradigm for RIα signaling and targeting through AKAP-mediated mechanisms.

Results

Punctate pattern of overexpressed RIα is RI specific

Type I PKA holoenzyme and free RIα are predominantly thought to be cytoplasmic; however, when we expressed GFP-tagged RIα in HeLa cells, we found a distinct punctate pattern (Fig. 1 A, top right). When we expressed RIα in RIα knockout MEFs (*Prkar1a*$^{-/-}$ MEFs), we saw a similar punctate pattern (Fig. 1 A, bottom right). In both cell lines, we observed the punctate pattern even when expression levels were low. To further confirm that puncta formation was not an artifact of overexpression, we used quantitative Western blot analysis to compare the levels of transfected RIα-GFP in *Prkar1a*$^{-/-}$ MEFs to endogenous levels of RIα in *Prkar1a*$^{+/+}$ MEFs (Fig. S1). Transfection efficiency of RIα-GFP in *Prkar1a*$^{-/-}$ MEFs was typically around 15–30%. Based on this efficiency and the difference in band intensities between RIα-GFP versus endogenous RIα (15.4-fold for experiment 1 and 18.1-fold for experiment 2), the expression levels of RIα-GFP with 100% transfection efficiency would range from 2.3- to 5.4-fold lower than the levels of endogenous RIα. Although these values are approximations, the results clearly demonstrate that RIα-GFP was not overexpressed in relation to the levels of endogenous RIα in *Prkar1a*$^{+/+}$ MEFs. In the remainder of this paper, the term "overexpression" is still used to indicate exogenous expression but is not indicative of the true levels of expression.

Four isoforms of the PKA R-subunits exist, and they display different localization patterns. We therefore next explored whether puncta formation was common to all R-subunits or unique to the RIα isoform. Constructs of the four R-subunit isoforms were expressed in HeLa cells and *Prkar1a*$^{-/-}$ MEFs (Fig. 1 B).

Published April 18, 2011

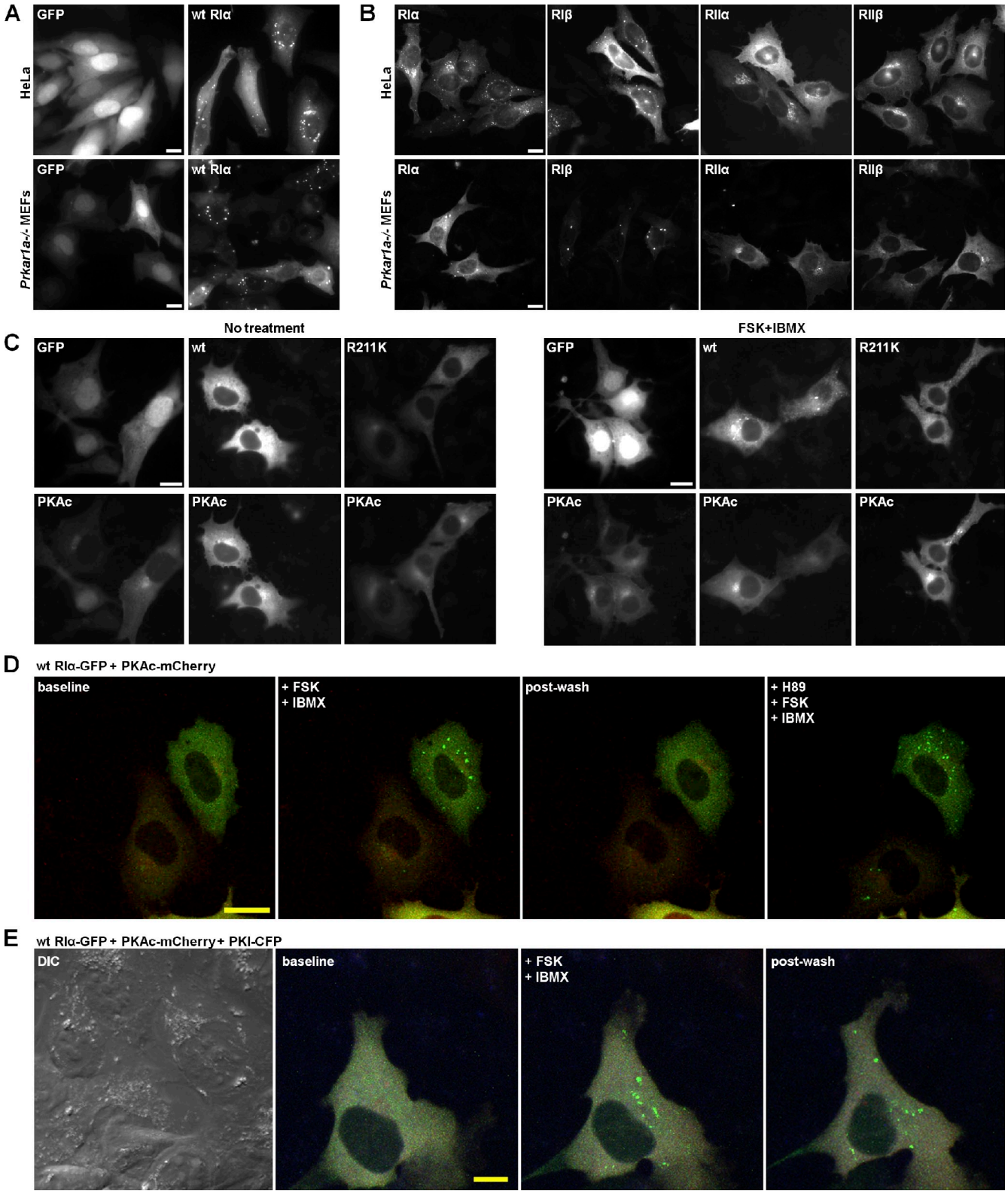

Figure 1. **Expression of wild-type RIα in mammalian cells revealed a punctate pattern that is RI specific.** (A) Transient transfection of control GFP empty vector or GFP-tagged RIα in HeLa cells (top) and *Prkar1a*$^{-/-}$ MEFs (bottom). (B) Expression of fluorescently tagged R-subunit isoforms in HeLa cells (top) and *Prkar1a*$^{-/-}$ MEFs (bottom). (C) Coexpression of control GFP empty vector or GFP-tagged RIα with mCherry-tagged PKAc in *Prkar1a*$^{-/-}$ MEFs without treatment (left) and with 20 µM forskolin/200 µM IBMX treatment (right). Labels in the top left corner of each image indicate which protein is observed. (D) Representative frames from Video 1 showing *Prkar1a*$^{-/-}$ MEFs transiently transfected with GFP-tagged RIα (green) and mCherry-tagged PKAc (red). 10 µM H89 was added to inhibit PKAc activity (last representative frame). (E) Representative frames from Video 3 showing *Prkar1a*$^{-/-}$ MEFs transiently transfected with GFP-tagged RIα (green), mCherry-tagged PKAc (red), and CFP-tagged PKI (blue). (D and E) Baseline represents the cell before any treatment, whereas postwash represents the cell after removal of treatment. 20 µM forskolin/200 µM IBMX was added to activate PKAc. DIC, differential interference contrast. wt, wild type. FSK, forskolin. Bars, 20 µm.

Published April 18, 2011

Overexpression of the RI isoforms showed a punctate pattern, whereas overexpression of the RII isoforms produced perinuclear localization. Therefore, the punctate pattern was an RI isoform-specific phenotype but not unique to RIα.

Free RIα, but not the holoenzyme, is associated with punctate pattern

In normal resting cells, RIα is predominantly present as an inactive heterotetramer. It has been shown that free RIα and the RIα holoenzyme localize to discrete locations. We therefore wondered whether it was free RIα or the type I PKA holoenzyme that was forming puncta. To answer this question, we coexpressed GFP-tagged wild-type RIα with mCherry-tagged PKAc. When both RIα and PKAc were overexpressed in *Prkar1a*$^{-/-}$ MEFs, RIα localization was diffuse in the cytoplasm (Fig. 1 C, left). These results suggested that type I PKA holoenzyme did not form puncta.

To test whether the overexpressed RIα could be recruited to puncta after its disassociation from PKAc, cells were treated with forskolin/IBMX to elevate cAMP levels. Forskolin, by activating adenylyl cyclase, increases the intracellular levels of cAMP, whereas IBMX, a nonspecific inhibitor of phosphodiesterases, prevents its breakdown. cAMP binds to RIα and releases PKAc from the holoenzyme complex. Under these conditions, the punctate pattern appeared (Fig. 1 C, right). However, when RIα(R211K), which is defective in cAMP binding (Bubis et al., 1988; Herberg et al., 1996), was coexpressed with PKAc, no puncta were observed with or without forskolin/IBMX treatment. Therefore, formation of puncta appears to require free RIα. These results also confirm that overexpressed wild-type RIα did not readily recruit endogenous PKAc, unlike the overexpressed mutant, which binds to endogenous PKAc to form the holoenzyme (Fig. 1 C and see Fig. 5 B). Consistent with this data, overexpression of RIα(R211K) alone did not result in a punctate pattern (unpublished data).

Live-cell imaging demonstrates that puncta formation is reversible

To follow the formation of the puncta, we performed live-cell imaging experiments with *Prkar1a*$^{-/-}$ MEFs transiently transfected with RIα-GFP and PKAc-mCherry (Fig. 1 D and Video 1). After 18 h of transfection, the cells were equilibrated in Opti-MEM for 1 h and imaged live at 37°C on a confocal microscope. The cells were treated through two rounds of forskolin/IBMX with four washes of Opti-MEM in between treatments. Before treatment (baseline), both RIα and PKAc displayed a diffuse pattern. Within ∼2 min of the first treatment, RIα showed a punctate pattern. This phenotype was reversible as indicated by the diffuse pattern within 4 min after the washout of drugs (postwash). The diffuse pattern suggested a reassociation of RIα with PKAc. When the cells were treated with the second forskolin/IBMX treatment, the punctate pattern reappeared, which was also reversible when the drugs were washed away again (shown in Video 1 but not in Fig. 1 D).

In a separate experiment, when cells were treated with forskolin/IBMX for ∼1.5 h and then washed three times with Opti-MEM and left without drugs for ∼45 min, the punctate pattern diminished but never became fully diffuse. Then, the strong punctate pattern reappeared within ∼3 min of adding a second round of forskolin/IBMX. This result indicated that any diffuse pattern observed during postwash was not simply a result of targeting RIα for rapid degradation (Video 2).

Punctate pattern is independent of PKAc activity and irreversible in the presence of a protein kinase inhibitor (PKI)

Upon activation, PKAc is released to phosphorylate downstream substrates. We therefore wanted to determine whether PKAc activity was required for puncta formation. When the cells from Video 1 displayed a diffuse pattern after undergoing two rounds of forskolin/IBMX treatments and washes, an inhibitor of PKA, the ATP analogue H89, was added for 10 min. Then, a third round of forskolin/IBMX treatment was added. Despite inhibiting PKAc activity, puncta formation still occurred, proving that PKAc activity was not necessary (Fig. 1 D, last image).

Another inhibitor of PKAc is the heat-stable PKI. To further prove that the punctate pattern is independent of PKAc activity, cells were transfected with RIα-GFP, PKAc-mCherry, and PKI-CFP simultaneously (Fig. 1 E and Video 3). These cells were given one round of forskolin/IBMX treatment followed by four washes of Opti-MEM. At the beginning, the cells showed a diffuse pattern, and then upon treatment, they presented a punctate pattern. However, in this case, the punctate pattern was not reversible when the drugs were removed, which indicated the inability of RIα to reassociate with PKAc in the presence of PKI. Thus, although PKAc activity was not required for puncta formation, release of PKAc from the RIα holoenzyme was necessary.

Fractionation experiments of MEFs reveal a migration of free RIα to membranes

To establish whether the puncta corresponded to membranous organelles or to protein aggregates, fractionation experiments were implemented (Fig. 2 A). *Prkar1a*$^{+/+}$ MEFs were used to look at the migration of endogenous RIα. At basal levels of cAMP, the majority of RIα was in the cytosolic fraction. However, upon 60 min of forskolin/IBMX treatment, RIα showed a significant shift to the membrane fraction. Meanwhile, no change in PKAc levels was seen. Under these conditions, RIα and PKAc were not seen in the nuclear fraction. RIα was also not present in the cytoskeletal fraction, which included all residual proteins and protein aggregates. Markers for each fraction were used to verify equal sample loading and to confirm minimal cross-contamination during subcellular fractionation. We performed the same experiment with *Prkar1a*$^{-/-}$ MEFs, overexpressing both GFP-tagged RIα with mCherry-tagged PKAc (unpublished data). Likewise, an increase of RIα levels in the membrane fraction was observed after forskolin/IBMX treatment. These results confirmed that free RIα was migrating to membranes and that free RIα was not forming protein aggregates.

Colocalization experiments of RIα

To determine which possible membranous organelles were associated with free RIα, commercially available antibodies were

Published April 18, 2011

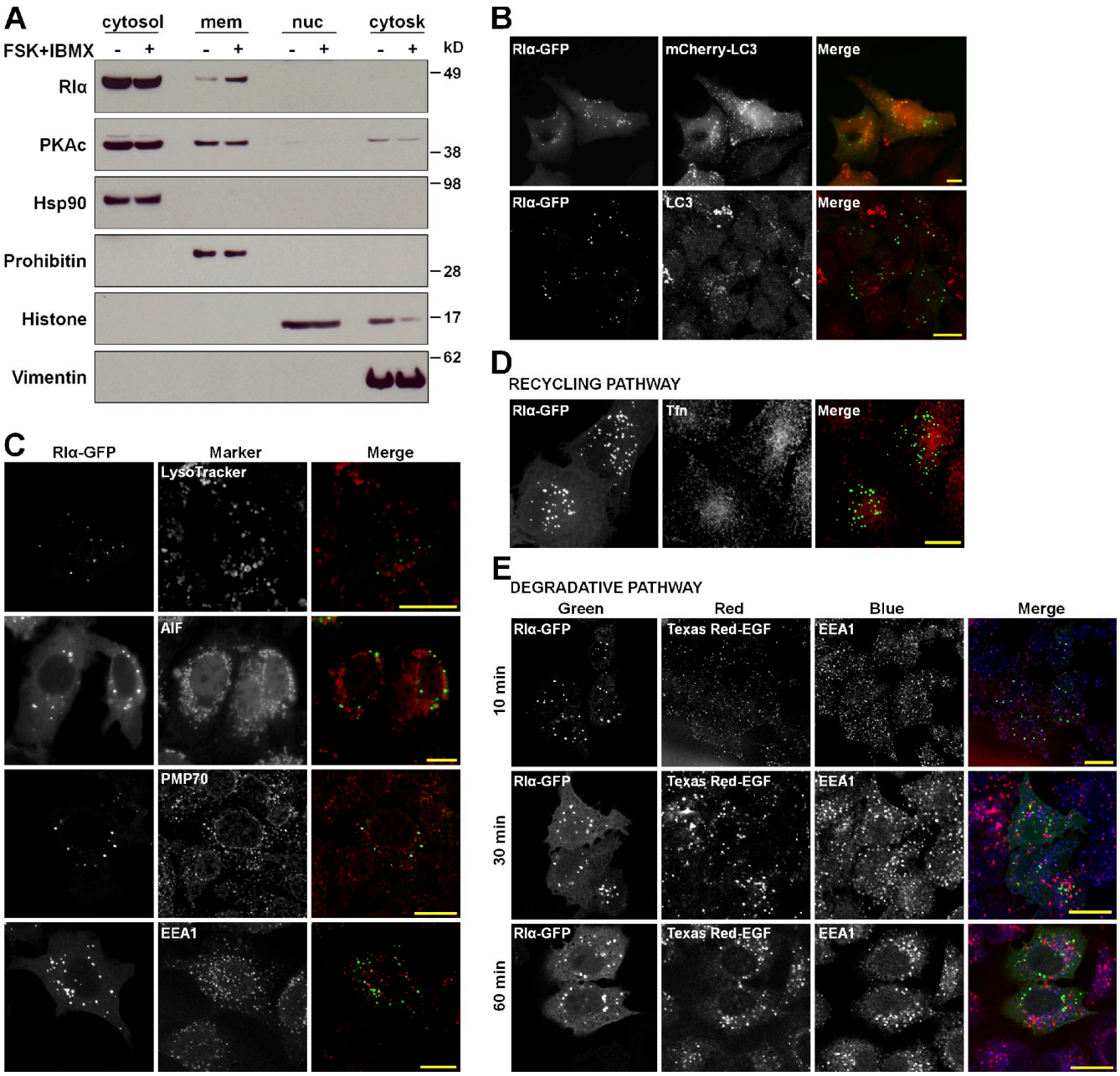

Figure 2. **Disassociated RIα localized to membranous organelles, and some organelles were ruled out from costaining with organelle markers.** (A) *Prkar1a*$^{+/+}$ MEFs were treated with 20 µM forskolin (FSK)/200 µM IBMX and fractionated. Cytosol refers to the cytosolic fraction, mem refers to the membrane fraction, nuc refers to the nuclear fraction, and cytosk refers to the cytoskeletal fraction. (B, top) HeLa cells were transiently cotransfected with GFP-tagged RIα (green) and mCherry-tagged LC3 (red). (bottom) Autophagy was induced in *Prkar1a*$^{-/-}$ MEFs, which were transiently transfected with GFP-tagged RIα (green), and then autophagosomes (LC3) were stained (red). (C) Cells were transfected with GFP-tagged RIα (green). *Prkar1a*$^{-/-}$ MEFs were stained for lysosomes (LysoTracker), mitochondria (AIF), and peroxisomes (PMP70), whereas HeLa cells were stained for early endosomes (EEA1). (D) Rhodamine-transferrin (Tfn) was used to follow the recycling pathway. (E) Texas red–EGF (EGF) was used to follow the degradative pathway, and cells were fixed at three different time points. EEA1 was stained so that a merge with EGF indicated early endosomes. Bars, 20 µm.

used to stain various organelles in *Prkar1a*$^{-/-}$ MEFs and HeLa cells (Fig. 2, B–E). Attempts to see the localization of free endogenous RIα were unsuccessful because of the lack of suitable antibodies for immunostaining RIα, thus we used RIα-GFP. Because it was previously reported that RIα colocalized with autophagosomes (Mavrakis et al., 2006), these were the first organelles we checked. However, when we coexpressed RIα-GFP with light chain 3 (LC3)–mCherry, we saw no colocalization (Fig. 2 B, top). Because transiently transfected LC3 can be incorporated into protein aggregates without actually labeling autophagosomes (Kuma et al., 2007), we also checked for colocalization by staining for LC3 after autophagy induction. Likewise, we saw no evidence of colocalization between RIα and endogenous LC3 (Fig. 2 B, bottom). Colocalization with lysosomes (LysoTracker) or mitochondria (apoptosis-inducing factor [AIF]) was also not observed (Fig. 2 C). When staining for peroxisomes using 70-kD peroxisomal membrane protein (PMP70), we found a partial overlap with GFP-tagged RIα in

Published April 18, 2011

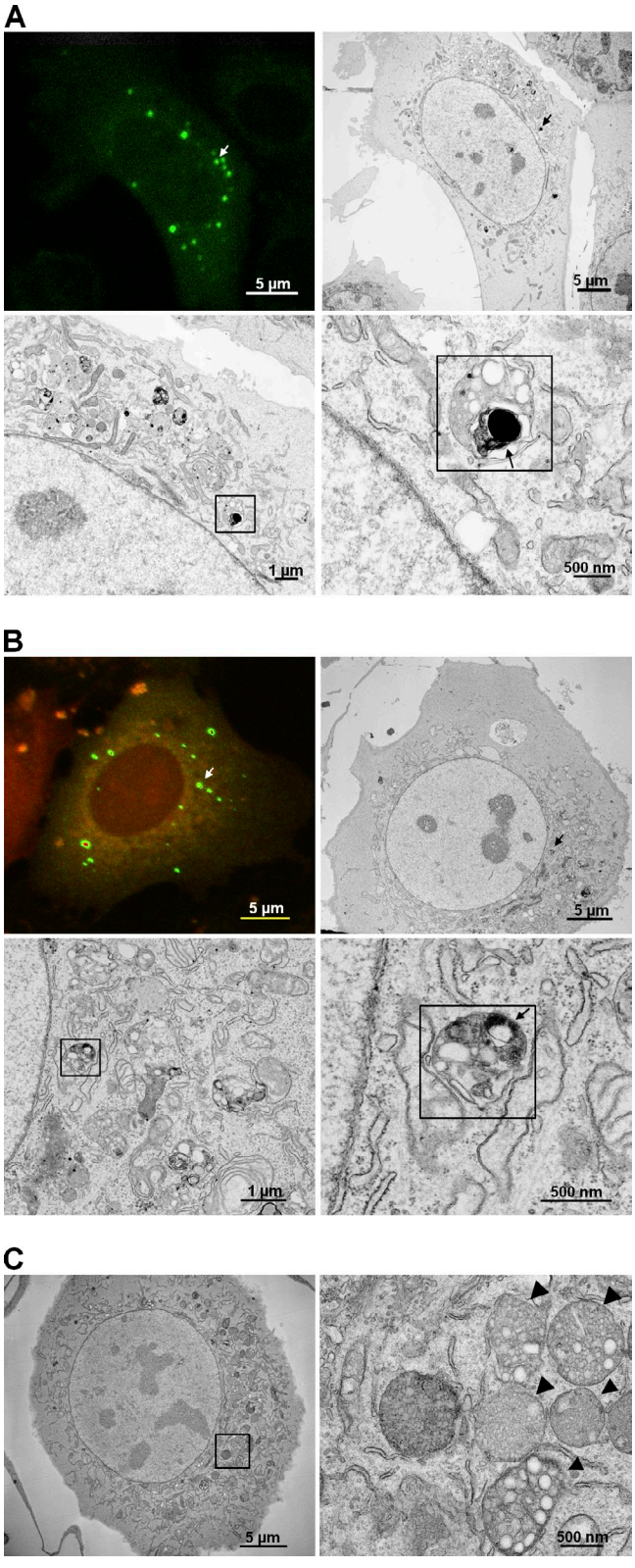

Figure 3. **Ultrastructural analysis revealed localization of RIα-GFP in MVBs.** Light and electron microscopy pictures were correlated to look for the localization of GFP-tagged RIα. (A and B, top) White/black arrows point to an MVB that was correlated. (bottom) The MVB is indicated by black squares. (bottom right) RIα-GFP is the dark black area within the MVB indicated by a black arrow. (A) *Prkar1a*$^{-/-}$ MEFs were transfected with RIα-GFP (green). (B) *Prkar1a*$^{-/-}$ MEFs were cotransfected with RIα-GFP (green) and PKAc-mCherry (red) and treated with 20 µM forskolin/200 µM IBMX. (C) Untransfected *Prkar1a*$^{-/-}$ MEFs were treated with 20 µM forskolin/200 µM IBMX. An enlarged image of MVBs from within the black square is shown on the right. The MVBs are indicated by black arrowheads.

both *Prkar1a*$^{-/-}$ MEFs and HeLa cells (unpublished data) but not enough to suggest a localization limited to peroxisomes.

We also transiently transfected HeLa cells with GFP-tagged RIα and stained for early endosomes (early endosome antigen 1 [EEA1]; Fig. 2 C, bottom). No overlap was detected, though the puncta were similar in size to EEA1 speckles. They were also very close and almost touching but not overlapping. Because the puncta were in such close proximity to EEA1, we looked for colocalization along the endosomal pathway. The recycling pathway was marked using rhodamine-transferrin but no overlap was found (Fig. 2 D). A search for localization along the degradative pathway was achieved using Texas red–labeled EGF (Fig. 2 E). Cells were fixed at different time points after the uptake of EGF to follow the different stages of the endosomal pathway. A great amount of overlap between Texas red–EGF and EEA1 at 10 min indicated that EGF localized to the early endosomes at that time point. However, no overlap between RIα and EGF/EEA1 was seen, although close proximity was consistently observed.

Electron microscopy experiments reveal localization to MVBs

Because our immunostaining was unsuccessful in identifying the organelles to which RIα-GFP localized, we used correlated light and electron microscopy for an ultrastructural analysis. We transiently transfected *Prkar1a*$^{-/-}$ MEFs with either GFP-tagged RIα alone or GFP-tagged RIα and mCherry-tagged PKAc (Fig. 3, A and B, respectively). A poststain with lead was performed before imaging to enhance the visualization of cell membranes. With the transfection of RIα-GFP, we observed electron-dense particles in organelles, making antibody staining unnecessary. In both cases, we discovered a localization of RIα-GFP to membranous organelles that resembled MVBs. As a control, we also looked at untransfected *Prkar1a*$^{-/-}$ MEFs that were treated with forskolin/IBMX (Fig. 3 C). No electron-dense product was observed in the MVBs from these cells, further verifying that the aforementioned dark electron-dense material was correlated with RIα-GFP. Thus, we found the localization of RIα-GFP puncta to MVBs. However, this localization was not a mechanism for its rapid degradation because we observed puncta that remained despite reintroducing holoenzyme formation conditions in live-cell imaging (Video 2).

Localization to MVBs is not caused by ubiquitination

Because ubiquitination of proteins is used as a sorting signal to MVBs (Katzmann et al., 2001; Reggiori and Pelham, 2001), we wondered whether the RIα targeted to MVBs was ubiquitinated. The PEST sequence is one signal that is recognized by the ubiquitin machinery, and RIα has a potential PEST sequence in its linker region (Bergold et al., 1992) that has been correlated with its ubiquitination upon cAMP binding (Hegde et al., 1993). To test the involvement of this PEST sequence, we used a PEST

Published April 18, 2011

sequence predictor to determine that mutating the proline-rich region would remove it. If the PEST sequence were involved in the localization of RIα to MVBs, removing it would disrupt puncta formation. However, when we mutated the PEST sequence, the punctate pattern was still observed, indicating that the PEST sequence was not essential for targeting to MVBs (Fig. S2). In addition, mass spectrometry analysis of human embryonic kidney (HEK) 293 cells overexpressing wild-type RIα did not detect ubiquitination of RIα (unpublished data). We also saw no evidence of higher molecular weight ubiquitinated forms of RIα in any of our Western blot analyses.

Localization of puncta is through AKAP binding

To deduce which region of RIα was essential for puncta formation, we expressed two GFP-tagged truncation mutants, RIα(1–93) and RIα(93–381). RIα(1–93) includes the D/D domain, whereas RIα(93–381) includes the two cAMP-binding domains. A faint punctate pattern was observed with the RIα(1–93) construct but not with the RIα(93–381) construct (Fig. 4 A). Thus, the N-terminal part of RIα was necessary for the punctate pattern. Because RII anchoring to membranous organelles occurs via AKAP binding at the D/D domain, we next tested whether an AKAP was involved in the recruitment of RIα to MVBs.

Previously, it has been shown that several mutations in RIα reduced its binding to a dual-specific AKAP1, D-AKAP1, in vitro (Banky et al., 1998). We introduced one of these mutations (I27A) into *Prkar1a*$^{-/-}$ MEFs, and the punctate pattern disappeared (Fig. 4 B). This result provided evidence that formation of the RIα puncta required AKAP binding.

To test this theory further, GFP-tagged RIα was coexpressed in *Prkar1a*$^{-/-}$ MEFs with mCherry-tagged peptide disruptors of AKAP binding (Fig. 4 C). These disruptors were derived from the C terminus of a dual-specific AKAP, D-AKAP2(623–662), which contains the PKA-binding motif. Residues identified for isoform specificity in a previous study (Burns-Hamuro et al., 2003) were mutated to make RI or RII selectivity. Coexpressing wild-type RIα with the RI/RII-selective AKAP disruptor resulted in no change to the punctate pattern. On the other hand, coexpressing wild-type RIα with an RI-selective AKAP disruptor caused the punctate pattern to become diffuse. However, the punctate pattern remained in the presence of the RII-selective AKAP disruptor. Although it might have been expected that the punctate pattern would become diffuse in the presence of the RI/RII-selective AKAP disruptor, the lack of change is not surprising. Burns-Hamuro et al. (2003) reported that D-AKAP2 binds with greater affinity to RIIα versus RIα (K_d = 2.2 nM vs. 48 nM, respectively); therefore, the nonspecific disruptor could naturally be more selective for RIIα because of its higher affinity to RIIα. Collectively, these results supported the notion that an RIα-specific AKAP is involved in localizing RIα to MVBs.

Mass spectrometry analysis reveals AKAP11 as a binding partner to disassociated RIα

Because >50 AKAPs exist (Wong and Scott, 2004), we developed affinity methods and mass spectrometry techniques for an unbiased screen of RIα-interacting partners, including AKAPs. We used untransfected HEK 293 cells and HEK 293 cells that were stably expressing tandem affinity purification (TAP)–tagged RIα.

First, to validate the accuracy of our methods, cAMP resin was used on untransfected HEK 293 cells to find proteins that bind to all four R-subunit isoforms (Table I, first method). The cAMP resin was directly subjected to trypsin digestion instead of buffer elution because it proved difficult to elute RIα from the cAMP resin. The digested peptides were then analyzed by mass spectrometry, and we considered a result as a true positive if it had at least two unique peptides. Three R-subunit isoforms were identified: RIα, RIIα, and RIIβ. Two AKAPs were also identified: AKAP9 and AKAP1.

We also used cAMP to find proteins that bind to all four R-subunit isoforms in the presence of stably transfected wild-type RIα (Table I, second method). The proteins that were identified included the same three R-subunit isoforms: RIα, RIIα, and RIIβ. In this case, though, three AKAPs were identified: AKAP11, AKAP9, and AKAP5. However, it was not clear which R-subunit isoforms bind to these proteins.

Therefore, to detect proteins associated with RIα instead of the other isoforms, we used the TAP tag system, in which stably transfected TAP-tagged RIα was purified with streptavidin and calmodulin resins (Table I, third method). In this case, we expected to find RIα, PKAc, and any protein that would bind to either RIα or to the RIα holoenzyme. Cell lysates were first bound to streptavidin resin, and then binding proteins were eluted and bound to calmodulin resin. As with the cAMP resin, proteins were not eluted from the calmodulin resin because of difficulty in disassociating TAP-tagged proteins from these beads. Instead, we ran the protein-bound calmodulin resin on an SDS-PAGE gel to separate any calmodulin that was attached to the beads. The gel pieces were digested and analyzed by mass spectrometry to identify proteins. Out of the three AKAPs that were identified when using cAMP alone, only one was detected using this technique, AKAP11.

To mimic the scenario from our microscopy experiments, we used the TAP tag system followed by cAMP to disassociate any PKAc (Table I, fourth method). From this method, we pulled out proteins that bound directly to free TAP-tagged RIα. AKAP11 was the only AKAP detected, and the unique peptides covered almost the entire AKAP11 sequence (unpublished data). Therefore, our mass spectrometry results suggested that AKAP11 is the best AKAP candidate responsible for the targeting of RIα to MVBs. These results also demonstrated that binding of AKAP11 to RIα is very robust, as it survived multiple stringent washes. Complete mass spectrometry data for all proteins that were pulled out under the aforementioned conditions are included as supplemental tables (Table S1, Table S2, Table S3, and Table S4).

AKAP11 binds to RIα in its free or holoenzyme form

To independently validate the interaction between AKAP11 and RIα, we immunoprecipitated endogenous AKAP11 from untransfected HEK 293 cells using the AKAP11 antibody or rabbit

Published April 18, 2011

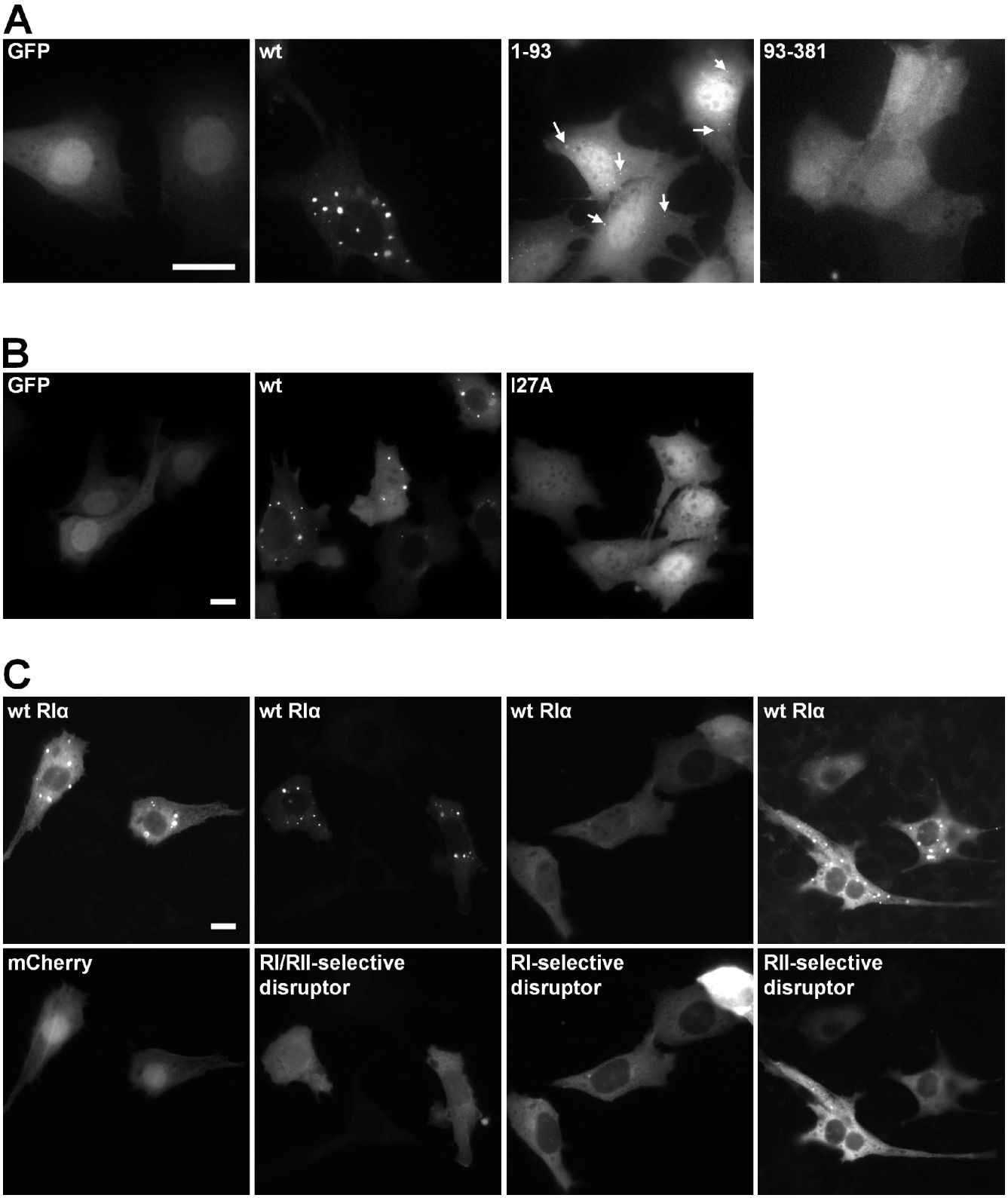

Figure 4. **Disruption of AKAP binding removed the punctate pattern.** (A) Control GFP empty vector, GFP-tagged wild-type (wt) RIα, and GFP-tagged deletion mutants, RIα(1–93) and RIα(93–381), were expressed in *Prkar1a*$^{-/-}$ MEFs. White arrows indicate a few of the faint puncta that were seen with the expression of RIα(1–93)-GFP. (B) A mutation that has been reported to disrupt D-AKAP1 binding, RIα(I27A), was GFP-tagged and expressed in *Prkar1a*$^{-/-}$ MEFs. GFP empty vector and GFP-tagged wild-type RIα were included as controls. (C) mCherry empty vector or mCherry-tagged AKB domain from D-AKAP2 (RI/RII selective, RI selective, or RII selective) was coexpressed with GFP-tagged RIα in *Prkar1a*$^{-/-}$ MEFs. Bars, 20 µm.

Published April 18, 2011

Table I. **cAMP-binding proteins and AKAPs identified from mass spectrometry using different purification methods on HEK 293 cell lysates**

Method/cell type	Protein description	IPI	Number of hits	Unique peptides
cAMP resin/untransfected	PKA type I-α R-subunit	IPI00021831	64	19
	PKA type II-α R-subunit	IPI00219774	104	31
	PKA type II-β R-subunit	IPI00554752	6	4
	AKAP9	IPI00019223	148	70
	AKAP1	IPI00022585	9	5
cAMP resin/stably transfected TAP-tagged wild-type RIα	PKA type I-α R-subunit	IPI00021831	57	19
	PKA type II-α R-subunit	IPI00219774	15	12
	PKA type II-β R-subunit	IPI00554752	9	6
	AKAP11	IPI00007411	9	8
	AKAP9	IPI00220628	5	4
	AKAP5	IPI00307794	2	2
Streptavidin and calmodulin resins/stably transfected TAP-tagged wild-type RIα	PKA type I-α R-subunit	IPI00021831	434	29
	PKA α–catalytic subunit	IPI00217960	2	2
	PKA α–catalytic subunit	IPI00396630	6	3
	AKAP11	IPI00007411	13	9
Streptavidin and cAMP resins/stably transfected TAP-tagged wild-type RIα	PKA type I-α R-subunit	IPI00021831	721	63
	PKA type I-β R-subunit	IPI00787996	21	14
	AKAP11	IPI00007411	113	59

IPI, International Protein Index.

IgG as a negative control. Samples were analyzed by Western blotting using antibodies for RIα, PKAc, and AKAP11 (Fig. 5 A). AKAP11 bound to both the RIα holoenzyme and free RIα. Inversely, we immunoprecipitated FLAG-tagged constructs of RIα that were transiently transfected into HEK 293 cells. As mentioned earlier, one mutation, RIα(R211K), is defective in cAMP binding. Samples were analyzed by Western blotting using antibodies for AKAP11, PKAc, and FLAG (Fig. 5 B). Both wild-type and mutant RIα interacted with AKAP11. As expected, a lower amount of PKAc was purified with wild-type RIα versus RIα(R211K) because RIα(R211K) would remain in complex with PKAc, despite the basal levels of cAMP. Together with the mass spectrometry data, this information led us to deduce that AKAP11 binds tightly to both free RIα and RIα in complex with PKAc.

We also demonstrated the colocalization of AKAP11 with RIα through immunofluorescence. HeLa cells and *Prkar1a*$^{-/-}$ MEFs were transiently transfected with RIα-GFP and stained for endogenous AKAP11. As observed from Fig. 5 C, the punctate pattern of AKAP11 overlapped with a majority of the punctate pattern from RIα-GFP, further suggesting their interaction at MVBs.

AKAP11 is responsible for the targeting of free RIα

Because we ascertained that AKAP11 binds to RIα and that free RIα, but not the holoenzyme, is targeted to MVBs, we next confirmed the colocalization of AKAP11 with RIα that was disassociated from PKAc. *Prkar1a*$^{-/-}$ MEFs were transiently transfected with RIα-GFP and PKAc-mCherry. One set of cells was left untreated (Fig. 6 A), whereas the other set was treated with forskolin/IBMX (Fig. 6 B). Then, both sets were stained for endogenous AKAP11. Before treatment, AKAP11 showed a diffuse pattern. After treatment, AKAP11 displayed a punctate pattern that overlapped with a majority of the RIα-GFP puncta.

Because AKAP11 displayed a punctate pattern only if RIα were punctate, we next addressed the question of whether AKAP11 is responsible for the targeting of RIα to form puncta. If this were the case, knocking down AKAP11 by RNA interference should have an effect on the targeting of RIα to MVBs. We thus treated *Prkar1a*$^{-/-}$ MEFs for 1–2 d with siRNA directed against AKAP11 and observed that siRNA effectively knocked down nearly all of the endogenous protein (Fig. 6 C). After 1 d of siRNA treatment, cells were transfected with wild-type RIα-GFP and analyzed through Western blotting and fluorescence microscopy analysis. We observed that the levels of RIα-GFP were unaffected by the knockdown of AKAP11 (Fig. 6 C); however, cells knocked down for AKAP11 no longer displayed a punctate pattern of RIα-GFP (Fig. 6 D). Collectively, these data suggest that AKAP11 is responsible for the targeting of free RIα to MVBs.

We thus propose a model for the targeting of free RIα that is blocked by the formation of the holoenzyme or by the disruption of AKAP binding and is independent of PKAc activity (Fig. 7). According to this model, AKAP11 is associated with the RIα holoenzyme when it is diffuse in the cytoplasm, and release of PKAc is required for recruitment of RIα to MVBs. Thus, holoenzyme formation not only inhibits the catalytic activity of PKAc but also prevents the targeting of free RIα to MVBs.

Discussion

Although the initial driving force for this study was to characterize the distinct puncta that formed when the free RIα subunit was expressed in mammalian cells, the finding that both free RIα and the RIα holoenzyme were associated with AKAP11 was another important discovery. Whereas RII subunits are constitutively localized to discrete areas in the cell through their tight binding to AKAPs, the RIα subunits are typically diffuse in the cytoplasm and only recruited to specific sites in response

Published April 18, 2011

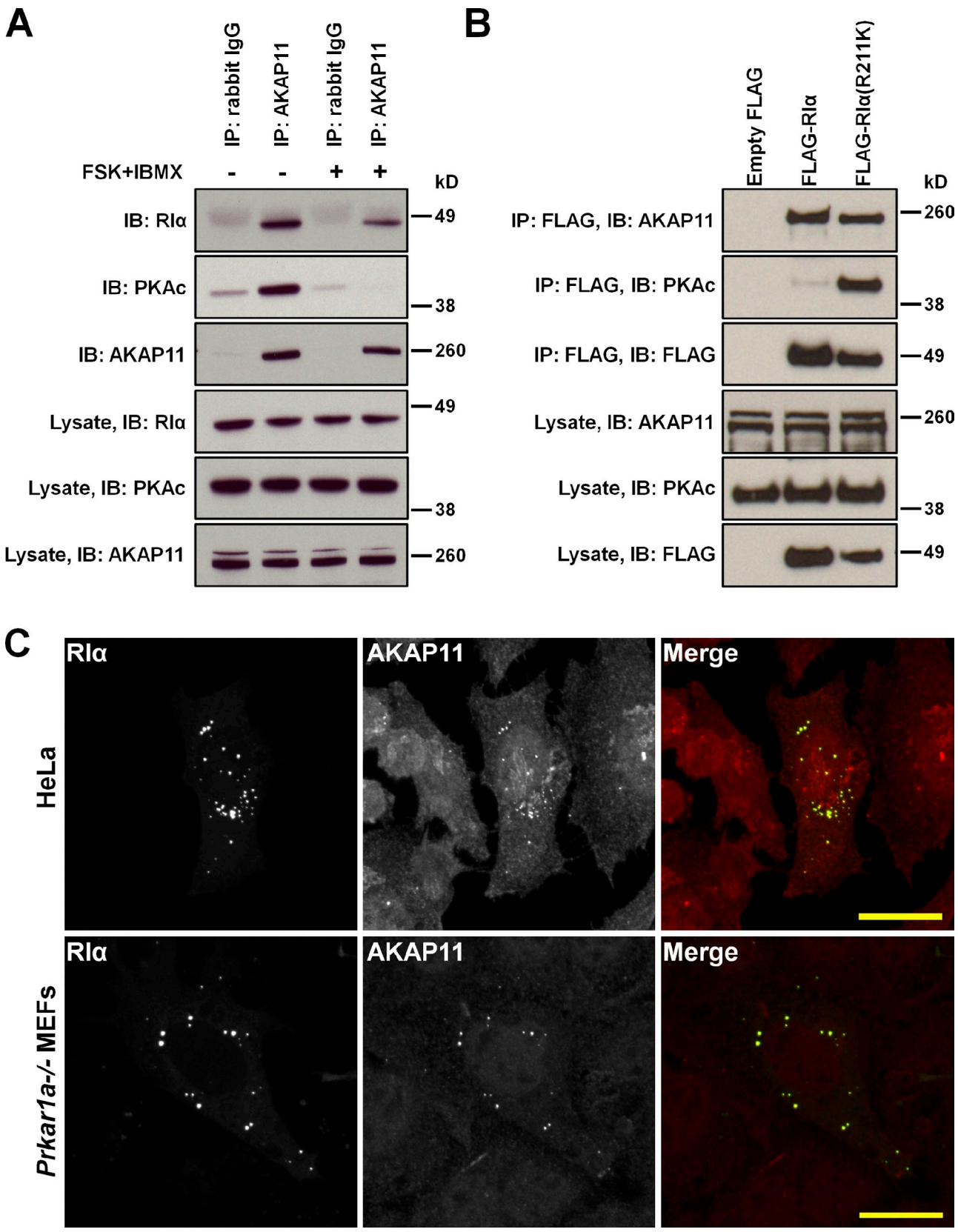

Figure 5. **AKAP11 binds to free RIα and the RIα holoenzyme.** (A) Endogenous AKAP11 was immunoprecipitated from HEK 293 cells in the absence and presence of 20 µM forskolin (FSK)/200 µM IBMX. Samples from the lysate and from the elution of the immunoprecipitation (IP) were immunoblotted (IB) with antibodies against RIα, PKAc, or AKAP11. (B) HEK 293 cells were transiently transfected with control FLAG empty vector, FLAG-tagged RIα, or FLAG-tagged RIα(R211K), an RIα mutant that is defective in cAMP binding. Samples from the lysate and from the elution of the IP were immunoblotted with antibodies against AKAP11, PKAc, or FLAG. (A and B) The lanes marked Lysate were loaded with 5% of the total cell lysates. (C) HeLa cells and *Prkar1a*$^{-/-}$ MEFs were transiently transfected with GFP-tagged RIα (green) and stained for endogenous AKAP11 (red). Bars, 20 µm.

Published April 18, 2011

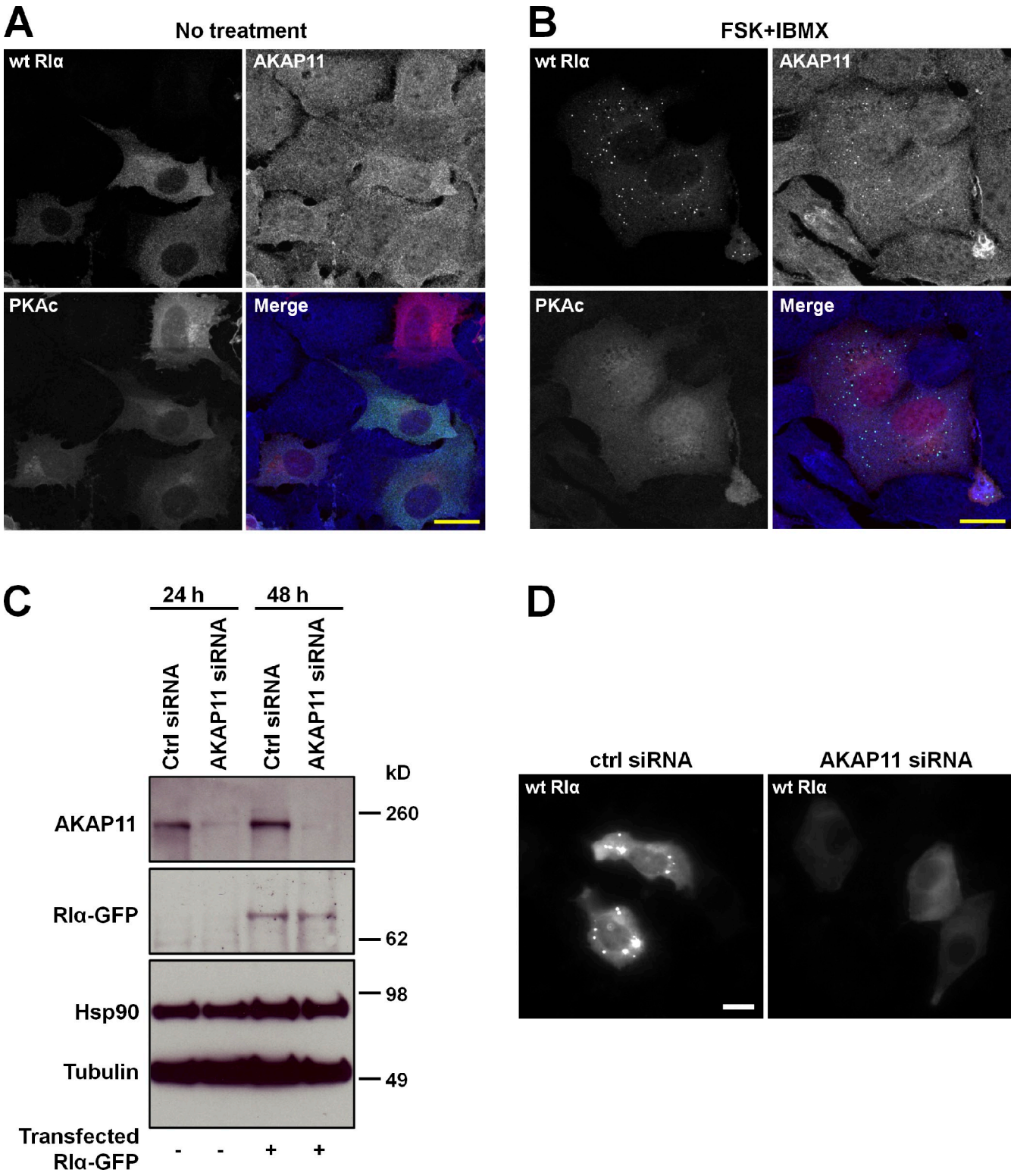

Figure 6. **AKAP11 targets free RIα.** (A) *Prkar1a*$^{-/-}$ MEFs were transiently cotransfected with GFP-tagged RIα (green) and mCherry-tagged PKAc (red) and stained for endogenous AKAP11 (blue). (B) *Prkar1a*$^{-/-}$ MEFs were transiently cotransfected with GFP-tagged RIα (green) and mCherry-tagged PKAc (red), treated with 20 µM forskolin (FSK)/200 µM IBMX, and then stained for endogenous AKAP11 (blue). (C) siRNA of AKAP11 effectively knocked down the levels of endogenous AKAP11 protein in *Prkar1a*$^{-/-}$ MEFs after 1–2 d. No effect on the expression level of transiently transfected RIα-GFP was observed, as judged by immunoblotting of whole-cell extracts with antibodies against AKAP11, RIα, Hsp90, or tubulin. (D) Knockdown of endogenous AKAP11 disrupted the formation of RIα-GFP puncta in *Prkar1a*$^{-/-}$ MEFs. Ctrl, control. wt, wild type. Bars, 20 µm.

Published April 18, 2011

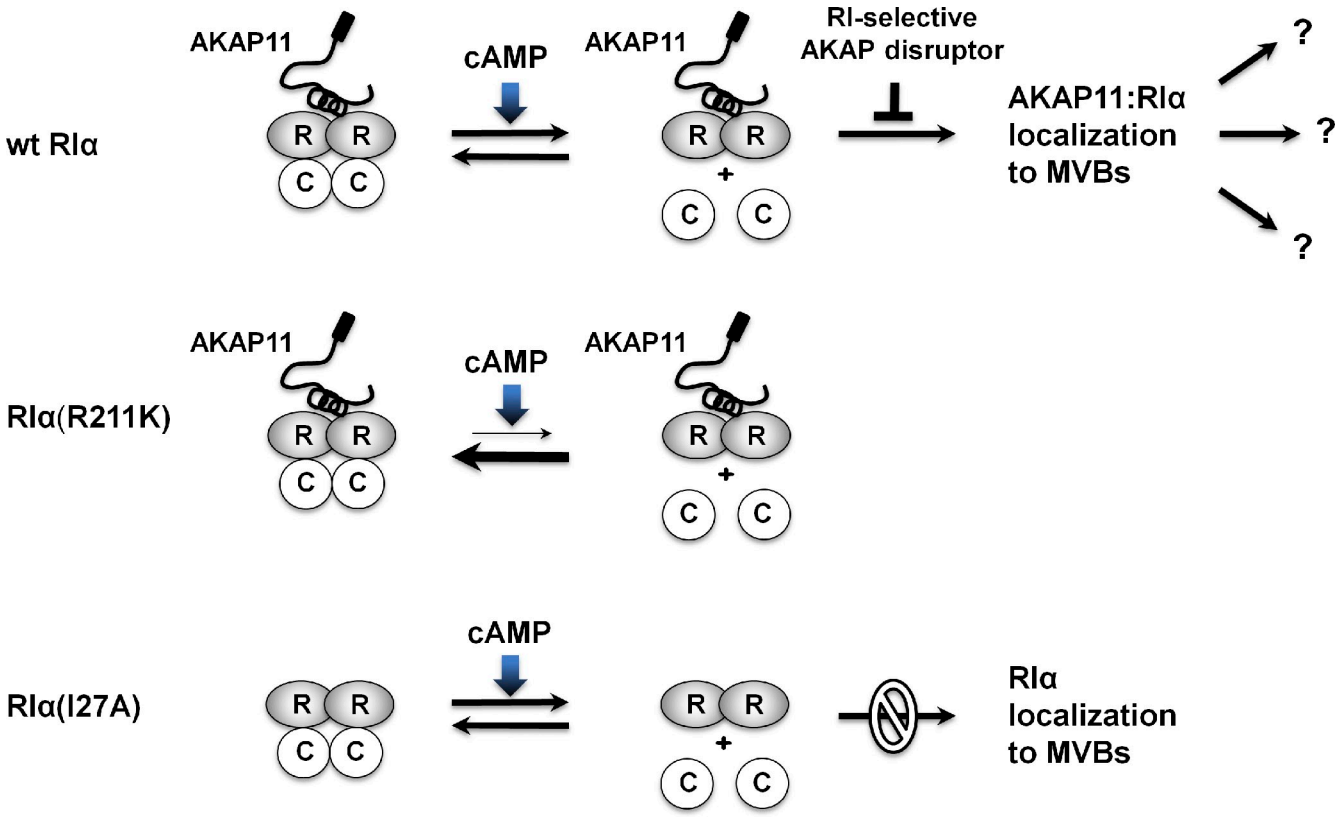

Figure 7. **Free RIα is recruited to MVBs by AKAP11.** A model for the mechanism of targeting RIα is depicted. AKAP11 binds to the RIα holoenzyme. Upon activation of PKA, AKAP11 stays bound to RIα, which is recruited to multivesicular bodies (MVBs). If the RIα holoenzyme is not activated, as in the case of RIα(R211K):PKAc, RIα does not get targeted. Likewise, free RIα is not targeted properly when AKAP11 binding is disrupted, as in the case with the RIα(I27A) mutation or in the presence of RI-selective AKAP disruptors. R, RIα; C, PKAc; wt, wild type.

to stimuli, for example, through the activation of T lymphocytes (Levy et al., 1996) or addition of hydrogen peroxide (Brennan et al., 2006). Here, we show that the association of RIα with AKAP11 defines a novel signaling mechanism for the RIα subunit that is distinct from the RII subunits and separate from its function as a regulator of PKAc.

We disproved several of the conclusions from an earlier study that analyzed RIα-GFP in cells (Mavrakis et al., 2006). Our data refuted their study of RIα localization to autophagosomes. Additionally, Mavrakis et al. (2006) claimed a statistically significant difference in the number of autophagosomes observed between *Prkar1a*$^{+/+}$ MEFs and *Prkar1a*$^{-/-}$ MEFs, which is contradictory to our data. Analysis of the number of autophagosomes as correlated by their volume density in the cytoplasm at the electron microscopy level produced no statistically significant difference in the number of autophagosomes between *Prkar1a*$^{+/+}$ MEFs and *Prkar1a*$^{-/-}$ MEFs (volume density is 1.5 and 1.4%, respectively). From looking at the number of autophagosomes in *Prkar1a*$^{-/-}$ MEFs at the light microscopy level, we discovered that cells with RIα-GFP puncta displayed lower induction of autophagy compared with cells without RIα-GFP puncta (representative picture in Fig. 2 B, bottom merge). Therefore, we conclusively proved that RIα was not colocalizing with autophagosomes, and the loss of RIα did not affect the number of autophagosomes in cells.

Instead, our electron microscopy results revealed the localization of RIα to MVBs. MVBs can only be definitively identified at the ultrastructural level (Clague and Urbé, 2008), which could be the reason for our difficulty in detecting colocalization through immunostaining, although we consistently saw close proximity to endosomes. We also determined that localization to MVBs was unique to the free RIα subunit, independent of PKAc activity, and reversible by lowering intracellular levels of cAMP.

To elucidate the molecular basis for RIα targeting to MVBs, we used several strategies to pinpoint that it was the AKAP-binding site within the N terminus that was required and that the AKAP needed was AKAP11. Our analysis also identified AKAP11 as a highly selective AKAP for RIα. Surprisingly, only the free RIα subunit goes to MVBs, even though AKAP11 appears to be associated with both the holoenzyme and the dissociated RIα subunit.

AKAP11, first discovered as an anchoring protein almost 15 yr ago (Lester et al., 1996), is a 220-kD protein that has been reported to bind to both RIα and RIIα in testis (Reinton et al., 2000); however, the interaction to RIα has not been studied in other cell lines, and its significance has never been addressed. In our experiments, we deduced that RIα(I27) was essential for binding with AKAP11 based on our mutagenesis experiments coupled with the recent structure of a D-AKAP2 peptide bound to RIα. In this structure, a mutation of RIα(I27) would affect

Published April 18, 2011

binding to an AKAP because it disrupts the packing of RIα(I35), a direct interactor to D-AKAP2 (Sarma et al., 2010). Most AKAPs with dual specificity have a 25–100-fold greater affinity for the RII versus RI isoforms (Herberg et al., 2000; Burns-Hamuro et al., 2003). Furthermore, the off rate of AKAPs with RIα is typically fast, making it difficult to analyze protein binding through RI overlay assays. In contrast, we find the binding of AKAP11 to RIα with our most stringent washes during purification (Fig. 5, A and B; and Table I), which led us to deduce the presence of a high affinity RIα-specific binding site in AKAP11. Three putative A-kinase binding (AKB) motifs exist in AKAP11 (Reinton et al., 2000). Based on the nature of the amphipathic helix that is formed from each of these putative AKB motifs and the recently predicted requirements for AKAP binding to RI versus RII subunits (Sarma et al., 2010), we predict that one of the AKB motifs has the potential to bind exclusively to RIα: AKAP11(611–628).

Although the precise role of targeting RIα to MVBs remains to be established, it does not appear to simply be a mechanism for degradation. Although MVBs were initially identified as part of the degradative pathway for proteins (Felder et al., 1990), it has now been discovered that MVBs also give rise to endosomal compartments that do not fuse with lysosomes, and subsequently, their cargo are not destined for degradation. For example, the major histocompatibility complex class II proteins accumulate in MVBs, but instead of being degraded, they are secreted from the cell upon fusion of the MVB with the plasma membrane (van Niel et al., 2006). Thus, MVBs can house proteins in temporary storage compartments without eventual degradation. We believe this is the case for the targeting of RIα to MVBs. Because we saw a reversibility of puncta formation, we suspect that the functionality of targeting RIα to MVBs is to keep RIα in a holding pattern until the holoenzyme reforms or its presence is needed somewhere else in the cell. A closer examination of our live-cell videos revealed that the puncta were merging with each other. The electron microscopy pictures showed that some of the electron-dense RIα-GFP appeared to be clinging to the MVB outer membrane, so it is possible that RIα is associated with the membrane from the cytosolic side, and not all were enclosed in the lumen. Furthermore, we do not believe that RIα is moving along the degradative pathway because of its lack of colocalization with lysosomes (Fig. 2 C, LysoTracker).

To our knowledge, this is the first study of RIα localizing to MVBs, and AKAP11 has never been shown to target there. In rats, AKAP11 potentially targets to peroxisomes because of the final three amino acids CRL (Lester et al., 1996), but human AKAP11 does not contain these final residues. We ruled out the targeting of human AKAP11 to peroxisomes because partial overlap of a couple of puncta, possibly caused by chance, was seen in only a few cells either stained for PMP70 or stained for proteins with another peroxisomal targeting sequence—SKL (unpublished data). Another study suggested the possibility of AKAP11 as an endosomal AKAP because of its colocalization with aquaporin 2 (AQP2) near apical membranes (Okutsu et al., 2008). AQP2 binds to AKAP11 (Okutsu et al., 2008) and is known to target to MVBs in kidney cells (Takata et al., 2008). Therefore, in HEK 293 or HeLa cells, the binding of AKAP11 to AQP2 may be the method by which the AKAP11:RIα complex is targeted to MVBs. AQP2 is not known to be expressed in MEFs, but in this cell line, another protein may be acting in a similar fashion to target AKAP11:RIα to MVBs. Elucidating the molecular basis for targeting AKAP11:RIα to MVBs is our next challenge.

Although other researchers have reported the association of RIα with proteins, such as RSK1 (p90 ribosomal S6 kinase; Chaturvedi et al., 2006), RFC40 (Gupte et al., 2005), and cytochrome *c* oxidase (Yang et al., 1998), we describe a unique signaling paradigm for the RIα subunit. Our model involves its dynamic and reversible recruitment to a specific organelle once it is disassociated from PKAc. We have known that the formation of the holoenzyme leads to the inactivation of PKAc, but we now discover that the holoenzyme also retains the RI subunit in a soluble signaling complex that prevents it from localizing to MVBs. The signaling complex, comprised of AKAP11 and RIα, is constitutively present, but the dynamic recruitment of RIα to MVBs requires the release of PKAc. AKAP11 has been suggested to regulate the cell cycle and play a role in driving oral carcinogenesis (Garnis et al., 2005), whereas RIα is involved in several different signaling pathways, cellular functions, and diseases. Therefore, it is likely that AKAP11 directs some of the RIα functions. Through our characterization of RIα puncta, we begin to have a handle on examining the fate of the disassociated RIα subunit, whether it is to compensate for excess PKAc levels, bind to other proteins to necessitate their translocation, or participate in the control of cell cycle and cell growth.

Materials and methods

Antibodies

The following antibodies were used for Western blot analysis: anti–RIα (Transduction Laboratories), anti-PKAc (Transduction Laboratories), anti-Hsp90 (Transduction Laboratories), antiprohibitin (Abcam), antihistone (Cell Signaling Technology), antivimentin (Abcam), anti-AKAP11 (generated by the laboratory of J. Scott, University of Washington, Seattle, WA), anti-AKAP11 (Abnova), anti–FLAG M2 (Sigma-Aldrich), and antitubulin (Sigma-Aldrich).

Cloning and expression of RIα and other proteins

Human RIα was subcloned from pCMV-SPORT6 (Invitrogen) into the HindIII–KpnI site of the pEGFP C2 vector (Takara Bio Inc.) and into the BamHI–HindIII site of the pNTAP vector (Agilent Technologies). Single site mutations were made in the full-length sequence by QuikChange mutagenesis (Agilent Technologies). Truncated RIα(1–93 and 93–381) was isolated by PCR, and the amplified cDNA was subcloned. Vectors for expression of mCherry- and FLAG-tagged proteins were generated as previously described (Eggers et al., 2009). RIα was subcloned into the HindIII–KpnI site of a FLAG vector. D-AKAP2 constructs were subcloned into the EcoRI–XhoI site of the mCherry vector. All constructs were verified by sequencing. R-subunit isoforms cloned into A-kinase activity reporter vectors were provided by F. Ma (University of California, San Diego, La Jolla, CA). PKAc tagged with mCherry and PKI tagged with CFP were provided by R. Tsien (University of California, San Diego, La Jolla, CA). LC3 tagged with mCherry was provided by A. Gustafsson (San Diego State University, San Diego, CA).

Cell lines and culture conditions

HeLa cells were obtained from the American Type Culture Collection. MEFs, immortalized by transformation with pBRSV encoding the SV40 virus, were provided by G.S. McKnight (University of Washington, Seattle, WA) and M. Ginsberg (University of California, San Diego, La Jolla, CA). Cells were maintained in DME supplemented with 10% fetal bovine serum (HyClone), 2 mM GlutaMax (Invitrogen), and 100 U/ml penicillin

Published April 18, 2011

and streptomycin (Invitrogen) under 8% CO_2. Transfections were performed with transfection reagent (Fugene 6; Roche) 1 d before imaging or with Lipofectamine 2000 (Invitrogen) 1 d before immunoprecipitation (IP). Stable cell lines of HEK 293 cells were generated by transfection with Lipofectamine 2000, selected accordingly for geneticin resistance, and maintained as described for HeLa cells and MEFs with the addition of 500 µg/ml geneticin (Invitrogen) to the media.

Live-cell imaging

Prkar1a$^{-/-}$ MEFs were grown overnight on poly-D-lysine–coated glass-bottom dishes (MatTek) and cotransfected with GFP-tagged RIα and mCherry-tagged PKAc (Fig. 1 D, Video 1, and Video 2) or cotransfected with GFP-tagged RIα, mCherry-tagged PKAc, and CFP-tagged PKI (Fig. 1 E and Video 3). 18 h after transfection, DME growth media were replaced with Opti-MEM (Invitrogen). cAMP levels were elevated by the addition of 20 µM forskolin (Sigma-Aldrich) and 200 µM IBMX (Sigma-Aldrich) simultaneously at 37°C. PKA activity was inhibited by the addition of 10 µM H89 (Millipore). Live-cell imaging sessions were conducted in a heated (37°C), sealed, humidified, and CO_2-equilibrated environmental chamber (WeatherStation; Precision Control) paired with a confocal laser-scanning microscope (FluoView1000; Olympus). Images were collected using an oil immersion 60× objective with an NA of 1.42 (Olympus). The data in Fig. 1 D, Video 1, and Video 2 were collected using 488- and 561-nm laser excitations, whereas the data in Fig. 1 E and Video 3 were collected using a 405-, 488-, and 561-nm laser excitations. Stacks of 25–30 slices (300-nm thick) were acquired using sequential scanning to prevent bleed through between channels. The collected volumes were processed using a customized ImageJ macro (written by O. Kwon, National Center for Microscopy and Imaging Research/Center for Research in Biological Systems, University of California, San Diego, La Jolla, CA) to generate a maximum intensity projection for each channel and time point and then merged into an AVI video.

Fractionation

Prkar1a$^{+/+}$ MEFs were grown on 15-cm Nunc dishes to ∼80% confluency. *Prkar1a*$^{-/-}$ MEFs were transfected using Lipofectamine 2000 and also grown to ∼80% confluency. One set was left untreated, whereas the other set was treated with 20 µM forskolin simultaneously with 200 µM IBMX for 1 h at 37°C. Cells were harvested in 2 ml of cold PBS and fractionated with a cell compartment kit (Qproteome; QIAGEN). Western blots were run on samples using equal volume loads. All primary antibodies were used at a dilution of 1:1,000 except for anti-Hsp90 (1:2,000 dilution) and antiprohibitin (1:100 dilution).

Immunofluorescence

HeLa cells and *Prkar1a*$^{-/-}$ MEFs were grown overnight in poly-D-lysine–coated glass-bottom dishes or on glass coverslips (Thermo Fisher Scientific), transfected with GFP-tagged RIα for 18–24 h, and fixed with 4% paraformaldehyde (Electron Microscopy Sciences) for 15 min at room temperature. *Prkar1a*$^{-/-}$ MEFs, which were cotransfected with GFP-tagged RIα and mCherry-tagged PKAc, were left untreated or treated with 20 µM forskolin simultaneously with 200 µM IBMX for 1 h at 37°C and fixed through the same method as cells transfected with GFP-tagged RIα alone. All solutions used during the immunostaining were prepared in Dulbecco's PBS (Mediatech). The following antibodies were used at 1:100 dilutions: anti-LC3 (Cell Signaling Technology), anti-AIF (Cell Signaling Technology), anti-PMP70 (Sigma-Aldrich), anti-EEA1 (Cell Signaling Technology), anti-AKAP11 (generated by J. Scott, University of Washington, Seattle, WA), Cy5-labeled donkey anti–rabbit IgG antibodies (Jackson ImmunoResearch Laboratories, Inc.), and DyLight 649 (Jackson ImmunoResearch Laboratories, Inc.). LysoTracker (Invitrogen) was used to visualize lysosomes. Cells were permeabilized in 0.2% Triton X-100 (Sigma-Aldrich) for 5 min at room temperature and blocked in 2% BSA (Sigma-Aldrich) followed by sequential incubations in primary and secondary antibodies. The method for staining LC3 was slightly altered: cells were permeabilized in 0.05% Triton X-100 for 15 min and blocked in 3% BSA. When using LysoTracker, cells were incubated with a probe diluted in prewarmed DME (final concentration of 50 nM) for 1 h at 37°C before fixation. Fixed cells were viewed with either a microscope (Axiovert 200M; Carl Zeiss) equipped with an oil immersion 40× objective with an NA of 1.3 (Carl Zeiss) and an electron microscopy charge-coupled device camera (Cascade II:512; Photometrics) or with a confocal laser-scanning microscope (FluoView1000) equipped with an oil immersion 60× objective with an NA of 1.42. Epifluorescent images were acquired with MetaFluor software (Molecular Devices), whereas confocal images were acquired with FluoView ASW 1.7c software (Olympus). The collected confocal images were processed using ImageJ (Abramoff et al., 2004) to generate maximum intensity projection images (z = 30–40 slices; z step = 0.3 µm) and Photoshop (Adobe) to generate composite pictures.

Induction of autophagy

Autophagy was induced in cells by amino acid and glucose starvation using Earle's balanced salt solution (Invitrogen) for 4 h at 37°C. Two lysosomal inhibitors, 1 µM pepstatin A (EMD) and 10 µM EST (EMD), were used to prevent the degradation of LC3-II.

Endosomal pathway

Recycling pathway. HeLa cells transfected with RIα-GFP were serum starved in DME supplemented with 0.5% BSA for 2 h. Alexa Fluor 568 transferrin receptor (Invitrogen) was added to the cells at a final concentration of 50 µg/ml for 1 h at 37°C. Cells were washed once with cold PBS, once with cold stripping buffer (500 mM NaCl and 0.5% acetic acid, pH 3.0) for 45 s, and two more times with cold PBS. Cells were fixed with 4% paraformaldehyde for 15 min at room temperature.

Degradative pathway. HeLa cells transfected with RIα-GFP were serum starved in DME supplemented with 0.5% BSA for 6 h. Texas red–labeled EGF (Invitrogen), diluted in cold DME to a final concentration of 1 µg/ml, was added to the cells. Unbound EGF was removed by washing in cold PBS. Prewarmed DME was added to the cells, and different time points were taken by fixing cells with 4% paraformaldehyde for 15 min at room temperature.

Electron microscopy

Prkar1a$^{-/-}$ MEFs were grown on glass-bottom grid dishes. After 18 h of transfection (using Fugene 6), cells were fixed in 2% paraformaldehyde and 2.5% glutaraldehyde in 0.1 M sodium cacodylate buffer, pH 7.4, solution for 5 min at room temperature and then moved to ice for a duration of 30 min for optimal cell ultrastructural preservation. The cells were washed five times in ice-cold 0.1 M sodium cacodylate buffer, pH 7.4, and 3 mM calcium chloride, each taking 2 min, to remove excess aldehydes. Cells were viewed with a confocal microscope (MRC-1024; Bio-Rad Laboratories) using 488- and 568-nm laser excitations and a 40× water objective lens with an NA of 1.2 (confocal stacks of z = 37 slices; z step = 0.36 µm). A transmitted image was viewed with either a 10 or 20× objective lens to determine the grid location. Images were acquired using LaserSharp 2000 software (Bio-Rad Laboratories/Carl Zeiss). The cultured cells were postfixed in ice-cold 1% osmium tetroxide with 0.8% potassium ferrocyanide and 3 mM calcium chloride for 30 min, washed five times in double-distilled water for 2 min each to stop the osmium tetroxide reaction, and en bloc stained in ice-cold 2% uranyl acetate overnight to help increase membrane contrast. Afterward, the cultured cells were dehydrated in an ethanol series for 3 min each, starting with 20, 50, 70, and 90% ethanol on ice and ending with four changes of 100% ethanol at room temperature. The dehydrated cells were infiltrated in a 1:1 ratio of absolute ethanol to epoxy resin (Durcupan ACM; Electron Microscopy Sciences) for 30 min and then with three changes of epoxy resin (Durcupan ACM) for 1 h each. Finally, a fourth epoxy resin (Durcupan ACM) change was performed, and immediately, the dish was placed in a vacuum oven at 60°C to be polymerized for 48–72 h. After polymerization, the coverslip was removed from the dish, and plastic blocks were sawed out and glued onto dummy blocks. 80-nm ultrathin serial sections were prepared using an ultramicrotome (Reichert–Jung Ultracut E; American Optical Instrument Company) with a diamond knife (Diatome), and the sections were supported onto 200 mesh copper grids. The 80-nm sections were poststained in Sato's lead for 1 min, and the stained sections were imaged using an electron microscope (JEM-1200EX II; JEOL) at 80 kV.

Pull-down experiments

Untransfected and stable HEK 293 cells were grown on Nunc dishes and harvested at 80% confluency in PBS. Cells were lysed in 50 mM Tris, pH 7.0, 150 mM NaCl, 1 mM EDTA, and 1% NP-40 by three freeze-thaw cycles. Lysates were bound to 8-AEA ([2-aminoethylamino]adenosine)–cAMP resin, streptavidin and calmodulin resins, or streptavidin and 8-AEA–cAMP resin. 8-AEA–cAMP was purchased from BioLog. Proteins bound to streptavidin resin were eluted with streptavidin buffer, which contains biotin (Agilent Technologies). Mass spectrometry analyses of proteins bound to cAMP or calmodulin resins are described in the next section.

Proteomics analysis

Proteins bound to cAMP resin. Proteins pulled down with cAMP beads were resuspended in 0.1 M ammonium bicarbonate. Reduction and alkylation of the sample was performed by adding DTT to a final concentration of

Published April 18, 2011

2 mM, incubating at room temperature for 30 min, and then adding iodoacetamide to a final concentration of 4 mM and incubating at room temperature for 30 min in the dark. 0.5 µg trypsin was added to the beads and incubated at 37°C overnight. The sample was acidified with formic acid (final concentration of 5%) and then separated from the cAMP beads by microfuge centrifugation and dried in a speed vacuum. The dried peptides were resuspended in 10 µl of buffer A (5% acetonitrile and 0.1% formic acid) and analyzed by automated microcapillary liquid chromatography–tandem mass spectrometry. Fused-silica capillaries (100-µm inner diameter) were pulled using a CO_2 laser puller (P-2000; Sutter Instrument) to a 5-µm inner diameter tip and packed with 10 cm of 5-µm Magic C18 material (Agilent Technologies) using a pressure bomb. This column was then placed in line with a quaternary HPLC pump (1100 series; Agilent Technologies) equipped with an autosampler (1100 series). The column was equilibrated in buffer A, and the peptide mixture was loaded onto the column using the autosampler. The HPLC pump flowed at 100 µl/min, and the flow rate to the electrospray tip was reduced to ~200–300 nL/min by a split. The HPLC separation was provided by a gradient between buffer A and buffer B (90% acetonitrile and 0.1% formic acid). The HPLC gradient was held constant at 100% buffer A for 5 min after peptide loading followed by a 30-min gradient from 5% buffer B to 40% buffer B. The gradient was then switched from 40 to 80% buffer B over 5 min and held constant for 3 min. Finally, the gradient was changed from 80% buffer B to 100% buffer A over 1 min and then held constant at 100% buffer A for another 15 min. The application of a 1.8-kV distal voltage electrosprayed the eluted peptides directly into the ion trap mass spectrometer (LTQ; ThermoFinnigan) equipped with an electrospray ionization source (nanoLC; ThermoFinnigan). Full mass (tandem mass spectrometry) spectra were recorded on the peptides over a 400–2,000-mass/charge range followed by five tandem mass events sequentially generated in a data-dependent manner on the first-, second-, third-, fourth-, and fifth-most intense ions selected from the full mass spectrometry spectrum (at 35% collision energy). Mass spectrometer scan functions and HPLC solvent gradients were controlled by a data system (Xcalibur; ThermoFinnigan).

Isolation of proteins bound to calmodulin resin. Proteins pulled down with calmodulin resin were run on a 4–12% Bis-Tris SDS-PAGE gel for 5 min. Gel bands were incubated with 20% acetonitrile in 0.1 M ammonium bicarbonate for 20 min and dehydrated with 100% acetonitrile. After drying, the gel pieces were resuspended in 1 mM DTT in 0.1 M ammonium bicarbonate and incubated for 30 min at room temperature. Next, 2 mM iodoacetamide was added, and samples were incubated for 30 min at room temperature. The supernatant was aspirated, and gel pieces were dehydrated with 100% acetonitrile. After drying, 250 ng trypsin was added in 0.1 M ammonium bicarbonate and incubated overnight. After incubation, the supernatant with the peptides was removed. The gel pieces were washed with 10% acetonitrile and 0.1% formic acid, and the washes were combined with the supernatant. This solution was dried in a speed vacuum, and the pellet was resuspended in 0.1% formic acid in 5% acetonitrile and loaded into the ion trap mass spectrometer (LTQ) as described in the methods for analyzing proteins bound to cAMP resin.

Data analysis. Tandem mass spectrometry spectra were extracted from the RAW file with ReADW.exe. The resulting mzXML file contained all the data for all tandem mass spectrometry spectra and was read by the subsequent analysis software. The tandem mass spectrometry data were searched with InsPecT (Tanner et al., 2005) against the human International Protein Index database v3.31 (Kersey et al., 2004) with optional modifications: +16 on methionine, +57 on cysteine, and +80 on threonine, serine, and tyrosine. Only peptides with a $P \geq 0.01$ were analyzed further.

Co-IPs

For endogenous AKAP11 co-IPs, HEK 293 cells were grown on 10-cm Nunc dishes to ~80% confluency. One set was left untreated, whereas the other set was treated with 20 µM forskolin simultaneously with 200 µM IBMX for 1 h at 37°C. A co-IP kit (Universal Magnetic; Active Motif) was used to perform whole-cell extractions and then to perform the co-IPs. Proteins were analyzed by Western blotting. For FLAG-RIα co-IPs, HEK 293 cells were grown in 10-cm dishes to ~80% confluency and transfected with FLAG plasmids. After 18–20 h, cells were harvested and lysed in a buffer (50 mM Tris, pH 7.0, 150 mM NaCl, 1 mM EDTA, and 1% NP-40) and bound to anti–Flag M2 affinity resin (Sigma-Aldrich) for 1 h at 4°C. Proteins that bound to the beads were eluted with SDS sample buffer and analyzed by Western blotting.

RNA interference

To knock down levels of AKAP11 with siRNA, *Prkar1a*$^{-/-}$ MEFs were transfected with 10 nM AKAP11 siRNA (siGENOME SMARTpool; Thermo Fisher Scientific) using Lipofectamine RNAiMAX (Invitrogen). The siGENOME nontargeting siRNA Pool #2 was used as a negative control. Cells were analyzed 1–2 d after siRNA treatment. Any transfection of plasmid DNA was performed 24 h after siRNA treatment.

Quantitative Western blot

Prkar1a$^{+/+}$ MEFs and *Prkar1a*$^{-/-}$ MEFs were grown to ~80% confluency on 10-cm Nunc dishes and transfected with empty GFP or GFP-tagged RIα, respectively. After 16–18 h, cells were harvested with cold CE1 buffer (10 mM Hepes, 60 mM KCl, 1 mM EDTA, 1 mM DTT, 1% BSA, and 0.5% NP-40) and lysed with sonication. Lysates were spun down at 14,000 rpm for 5 min. Proteins from the supernatant were analyzed by Western blotting. Band intensity levels were measured using the AlphaView Q software on an imaging system (FluorChem Q; Cell Biosciences, Inc.).

Stereology

The volume density of autophagosomes was determined using stereological observations similar to those previously described (Yuan et al., 2007) on electron microscopy images as follows. Point counting was used to determine the volume densities by overlaying a 100-point square grid on each digitized image (4,033 × 6,010 pixels with a pixel size of 2.8 nm) in Photoshop. Observations were made at the points of intersection (15 × 21 points) of the grid. First, the volume available for autophagosomes to occupy was counted on each image. This was accomplished by excluding those points lying on top of any nucleus present and any empty space, that is, space not occupied by the cytoplasm. Next, the points lying directly on top of autophagosomes were counted. The volume density of mitochondria was calculated by dividing the number of autophagosome points by the cytoplasm points.

Online supplemental material

Fig. S1 shows that puncta formation is not an artifact of RIα-GFP overexpression. Fig. S2 shows that ubiquitination of RIα is not the signal for targeting to MVBs. Video 1 shows that RIα puncta formation is reversible and independent of PKAc activity. Video 2 shows that RIα puncta is not rapidly degraded, and formation is reversible for up to 3 h. Video 3 shows that RIα puncta formation is not reversible in the presence of PKI. Table S1 lists the proteins identified to bind to all four R-subunit isoforms in untransfected HEK 293 cells. Table S2 lists the proteins identified to bind to all four R-subunit isoforms in HEK 293 cells that are stably expressing TAP-tagged RIα. Table S3 lists the proteins identified to bind to TAP-tagged RIα, which were free or in complex with PKAc, in HEK 293 cells that are stably expressing TAP-tagged RIα. Table S4 lists the proteins identified to bind to free TAP-tagged RIα in HEK 293 cells that are stably expressing TAP-tagged RIα. Online supplemental material is available at http://www.jcb.org/cgi/content/full/jcb.201010034/DC1.

We thank Christopher Eggers for useful discussions and valuable assistance with colocalization experiments along the endosomal pathway. We wish to thank Ohkyung Kwon for help with image processing and analysis and both Ohkyung and Hiroyuki Hakozaki for exceptional assistance with microscope setup. We also wish to thank Philip Chang for assistance with the analysis of RIαGFP expression levels. We greatly appreciate discussions with Hilde Abrahamsen regarding autophagy. We also thank Christopher Benner for careful reviews of manuscript drafts.

This work was supported by National Institutes of Health grants DK54441 to S.S. Taylor and J.D. Scott, P41-RR004050 to M.H. Ellisman, and a Ruth L. Kirschstein National Research Service Award NIH/NCI T32 CA009523 to M.E. Day.

Submitted: 6 October 2010
Accepted: 15 March 2011

References

Abramoff, M.D., P.J. Magelhaes, and S.J. Ram. 2004. Image processing with ImageJ. *Biophoton. Int.* 11:36–42.

Amieux, P.S., and G.S. McKnight. 2002. The essential role of RI alpha in the maintenance of regulated PKA activity. *Ann. NY Acad. Sci.* 968:75–95. doi:10.1111/j.1749-6632.2002.tb04328.x

Banky, P., L.J. Huang, and S.S. Taylor. 1998. Dimerization/docking domain of the type Ialpha regulatory subunit of cAMP-dependent protein kinase. Requirements for dimerization and docking are distinct but overlapping. *J. Biol. Chem.* 273:35048–35055. doi:10.1074/jbc.273.52.35048

Bergold, P.J., S.A. Beushausen, T.C. Sacktor, S. Cheley, H. Bayley, and J.H. Schwartz. 1992. A regulatory subunit of the cAMP-dependent protein kinase

down-regulated in aplysia sensory neurons during long-term sensitization. *Neuron*. 8:387–397. doi:10.1016/0896-6273(92)90304-V

Boeshans, K.M., K.A. Resing, J.B. Hunt, N.G. Ahn, and J.B. Shabb. 1999. Structural characterization of the membrane-associated regulatory subunit of type I cAMP-dependent protein kinase by mass spectrometry: identification of Ser81 as the in vivo phosphorylation site of RIalpha. *Protein Sci.* 8:1515–1522. doi:10.1110/ps.8.7.1515

Boshart, M., F. Weih, M. Nichols, and G. Schütz. 1991. The tissue-specific extinguisher locus TSE1 encodes a regulatory subunit of cAMP-dependent protein kinase. *Cell*. 66:849–859. doi:10.1016/0092-8674(91)90432-X

Brandon, E.P., M. Zhuo, Y.Y. Huang, M. Qi, K.A. Gerhold, K.A. Burton, E.R. Kandel, G.S. McKnight, and R.L. Idzerda. 1995. Hippocampal long-term depression and depotentiation are defective in mice carrying a targeted disruption of the gene encoding the RI beta subunit of cAMP-dependent protein kinase. *Proc. Natl. Acad. Sci. USA*. 92:8851–8855. doi:10.1073/pnas.92.19.8851

Brennan, J.P., S.C. Bardswell, J.R. Burgoyne, W. Fuller, E. Schröder, R. Wait, S. Begum, J.C. Kentish, and P. Eaton. 2006. Oxidant-induced activation of type I protein kinase A is mediated by RI subunit interprotein disulfide bond formation. *J. Biol. Chem.* 281:21827–21836. doi:10.1074/jbc.M603952200

Bubis, J., J.J. Neitzel, L.D. Saraswat, and S.S. Taylor. 1988. A point mutation abolishes binding of cAMP to site A in the regulatory subunit of cAMP-dependent protein kinase. *J. Biol. Chem.* 263:9668–9673.

Burns-Hamuro, L.L., Y. Ma, S. Kammerer, U. Reineke, C. Self, C. Cook, G.L. Olson, C.R. Cantor, A. Braun, and S.S. Taylor. 2003. Designing isoform-specific peptide disruptors of protein kinase A localization. *Proc. Natl. Acad. Sci. USA*. 100:4072–4077. doi:10.1073/pnas.2628038100

Burton, K.A., B. Treash-Osio, C.H. Muller, E.L. Dunphy, and G.S. McKnight. 1999. Deletion of type IIalpha regulatory subunit delocalizes protein kinase A in mouse sperm without affecting motility or fertilization. *J. Biol. Chem.* 274:24131–24136. doi:10.1074/jbc.274.34.24131

Chaturvedi, D., H.M. Poppleton, T. Stringfield, A. Barbier, and T.B. Patel. 2006. Subcellular localization and biological actions of activated RSK1 are determined by its interactions with subunits of cyclic AMP-dependent protein kinase. *Mol. Cell. Biol.* 26:4586–4600. doi:10.1128/MCB.01422-05

Chen, H.X., J.L. Marshall, E. Ness, R.R. Martin, B. Dvorchik, N. Rizvi, J. Marquis, M. McKinlay, W. Dahut, and M.J. Hawkins. 2000. A safety and pharmacokinetic study of a mixed-backbone oligonucleotide (GEM231) targeting the type I protein kinase A by two-hour infusions in patients with refractory solid tumors. *Clin. Cancer Res.* 6:1259–1266.

Clague, M.J., and S. Urbé. 2008. Multivesicular bodies. *Curr. Biol.* 18:R402–R404. doi:10.1016/j.cub.2008.02.068

Clegg, C.H., G.G. Cadd, and G.S. McKnight. 1988. Genetic characterization of a brain-specific form of the type I regulatory subunit of cAMP-dependent protein kinase. *Proc. Natl. Acad. Sci. USA*. 85:3703–3707. doi:10.1073/pnas.85.11.3703

Eggers, C.T., J.C. Schafer, J.R. Goldenring, and S.S. Taylor. 2009. D-AKAP2 interacts with Rab4 and Rab11 through its RGS domains and regulates transferrin receptor recycling. *J. Biol. Chem.* 284:32869–32880. doi:10.1074/jbc.M109.022582

Felder, S., K. Miller, G. Moehren, A. Ullrich, J. Schlessinger, and C.R. Hopkins. 1990. Kinase activity controls the sorting of the epidermal growth factor receptor within the multivesicular body. *Cell*. 61:623–634. doi:10.1016/0092-8674(90)90474-S

Garnis, C., M.P. Rosin, L. Zhang, and W.L. Lam. 2005. Alteration of AKAP220, an upstream component of the Rb pathway, in oral carcinogenesis. *Int. J. Cancer*. 116:813–819. doi:10.1002/ijc.21065

Goel, S., K. Desai, M. Macapinlac, S. Wadler, G. Goldberg, A. Fields, M. Einstein, F. Volterra, B. Wong, R. Martin, and S. Mani. 2006. A phase I safety and dose escalation trial of docetaxel combined with GEM231, a second generation antisense oligonucleotide targeting protein kinase A R1alpha in patients with advanced solid cancers. *Invest. New Drugs*. 24:125–134. doi:10.1007/s10637-006-2378-x

Gupte, R.S., Y. Weng, L. Liu, and M.Y. Lee. 2005. The second subunit of the replication factor C complex (RFC40) and the regulatory subunit (RIalpha) of protein kinase A form a protein complex promoting cell survival. *Cell Cycle*. 4:322–329. doi:10.4161/cc.4.2.1470

Hegde, A.N., A.L. Goldberg, and J.H. Schwartz. 1993. Regulatory subunits of cAMP-dependent protein kinases are degraded after conjugation to ubiquitin: a molecular mechanism underlying long-term synaptic plasticity. *Proc. Natl. Acad. Sci. USA*. 90:7436–7440. doi:10.1073/pnas.90.16.7436

Herberg, F.W., S.S. Taylor, and W.R. Dostmann. 1996. Active site mutations define the pathway for the cooperative activation of cAMP-dependent protein kinase. *Biochemistry*. 35:2934–2942. doi:10.1021/bi951647c

Herberg, F.W., A. Maleszka, T. Eide, L. Vossebein, and K. Tasken. 2000. Analysis of A-kinase anchoring protein (AKAP) interaction with protein kinase A (PKA) regulatory subunits: PKA isoform specificity in AKAP binding. *J. Mol. Biol.* 298:329–339. doi:10.1006/jmbi.2000.3662

Imaizumi-Scherrer, T., D.M. Faust, S. Barradeau, R. Hellio, and M.C. Weiss. 2001. Type I protein kinase a is localized to interphase microtubules and strongly associated with the mitotic spindle. *Exp. Cell Res.* 264:250–265. doi:10.1006/excr.2001.5164

Jahnsen, T., L. Hedin, V.J. Kidd, W.G. Beattie, S.M. Lohmann, U. Walter, J. Durica, T.Z. Schulz, E. Schiltz, M. Browner, et al. 1986. Molecular cloning, cDNA structure, and regulation of the regulatory subunit of type II cAMP-dependent protein kinase from rat ovarian granulosa cells. *J. Biol. Chem.* 261:12352–12361.

Jones, K.W., M.H. Shapero, M. Chevrette, and R.E. Fournier. 1991. Subtractive hybridization cloning of a tissue-specific extinguisher: TSE1 encodes a regulatory subunit of protein kinase A. *Cell*. 66:861–872. doi:10.1016/0092-8674(91)90433-Y

Kammer, G.M., I.U. Khan, J.A. Kammer, I. Olorenshaw, and D. Mathis. 1996. Deficient type I protein kinase A isozyme activity in systemic lupus erythematosus T lymphocytes: II. Abnormal isozyme kinetics. *J. Immunol.* 157:2690–2698.

Katzmann, D.J., M. Babst, and S.D. Emr. 2001. Ubiquitin-dependent sorting into the multivesicular body pathway requires the function of a conserved endosomal protein sorting complex, ESCRT-I. *Cell*. 106:145–155. doi:10.1016/S0092-8674(01)00434-2

Kersey, P.J., J. Duarte, A. Williams, Y. Karavidopoulou, E. Birney, and R. Apweiler. 2004. The International Protein Index: an integrated database for proteomics experiments. *Proteomics*. 4:1985–1988. doi:10.1002/pmic.200300721

Kirschner, L.S., J.A. Carney, S.D. Pack, S.E. Taymans, C. Giatzakis, Y.S. Cho, Y.S. Cho-Chung, and C.A. Stratakis. 2000. Mutations of the gene encoding the protein kinase A type I-alpha regulatory subunit in patients with the Carney complex. *Nat. Genet.* 26:89–92. doi:10.1038/79238

Kuma, A., M. Matsui, and N. Mizushima. 2007. LC3, an autophagosome marker, can be incorporated into protein aggregates independent of autophagy: caution in the interpretation of LC3 localization. *Autophagy*. 3:323–328.

Laxminarayana, D., I.U. Khan, N. Mishra, I. Olorenshaw, K. Taskén, and G.M. Kammer. 1999. Diminished levels of protein kinase A RI alpha and RI beta transcripts and proteins in systemic lupus erythematosus T lymphocytes. *J. Immunol.* 162:5639–5648.

Lee, D.C., D.F. Carmichael, E.G. Krebs, and G.S. McKnight. 1983. Isolation of a cDNA clone for the type I regulatory subunit of bovine cAMP-dependent protein kinase. *Proc. Natl. Acad. Sci. USA*. 80:3608–3612. doi:10.1073/pnas.80.12.3608

Lester, L.B., V.M. Coghlan, B. Nauert, and J.D. Scott. 1996. Cloning and characterization of a novel A-kinase anchoring protein. AKAP 220, association with testicular peroxisomes. *J. Biol. Chem.* 271:9460–9465. doi:10.1074/jbc.271.16.9460

Levy, F.O., A.M. Rasmussen, K. Taskén, B.S. Skålhegg, H.S. Huitfeldt, S. Funderud, E.B. Smeland, and V. Hansson. 1996. Cyclic AMP-dependent protein kinase (cAK) in human B cells: co-localization of type I cAK (RI alpha 2 C2) with the antigen receptor during anti-immunoglobulin-induced B cell activation. *Eur. J. Immunol.* 26:1290–1296. doi:10.1002/eji.1830260617

Lim, C.J., J. Han, N. Yousefi, Y. Ma, P.S. Amieux, G.S. McKnight, S.S. Taylor, and M.H. Ginsberg. 2007. Alpha4 integrins are type I cAMP-dependent protein kinase-anchoring proteins. *Nat. Cell Biol.* 9:415–421. doi:10.1038/ncb1561

Mavrakis, M., J. Lippincott-Schwartz, C.A. Stratakis, and I. Bossis. 2006. Depletion of type IA regulatory subunit (RIalpha) of protein kinase A (PKA) in mammalian cells and tissues activates mTOR and causes autophagic deficiency. *Hum. Mol. Genet.* 15:2962–2971. doi:10.1093/hmg/ddl239

McKnight, G.S., D.E. Cummings, P.S. Amieux, M.A. Sikorski, E.P. Brandon, J.V. Planas, K. Motamed, and R.L. Idzerda. 1998. Cyclic AMP, PKA, and the physiological regulation of adiposity. *Recent Prog. Horm. Res.* 53:139–159; discussion 160–161.

Miller, W.R. 2002. Regulatory subunits of PKA and breast cancer. *Ann. NY Acad. Sci.* 968:37–48. doi:10.1111/j.1749-6632.2002.tb04325.x

Okutsu, R., T. Rai, A. Kikuchi, M. Ohno, K. Uchida, S. Sasaki, and S. Uchida. 2008. AKAP220 colocalizes with AQP2 in the inner medullary collecting ducts. *Kidney Int.* 74:1429–1433. doi:10.1038/ki.2008.402

Orellana, S.A., and G.S. McKnight. 1990. The S49 Kin- cell line transcribes and translates a functional mRNA coding for the catalytic subunit of cAMP-dependent protein kinase. *J. Biol. Chem.* 265:3048–3053.

Reggiori, F., and H.R. Pelham. 2001. Sorting of proteins into multivesicular bodies: ubiquitin-dependent and -independent targeting. *EMBO J.* 20:5176–5186. doi:10.1093/emboj/20.18.5176

Reimann, E.M., D.A. Walsh, and E.G. Krebs. 1971. Purification and properties of rabbit skeletal muscle adenosine 3′,5′-monophosphate-dependent protein kinases. *J. Biol. Chem.* 246:1986–1995.

Reinton, N., P. Collas, T.B. Haugen, B.S. Skâlhegg, V. Hansson, T. Jahnsen, and K. Taskén. 2000. Localization of a novel human A-kinase-anchoring protein, hAKAP220, during spermatogenesis. *Dev. Biol.* 223:194–204. doi:10.1006/dbio.2000.9725

Rubin, C.S. 1979. Characterization and comparison of membrane-associated and cytosolic cAMP-dependent protein kinases. Studies on human erythrocyte protein kinases. *J. Biol. Chem.* 254:12439–12449.

Sarma, G.N., F.S. Kinderman, C. Kim, S. von Daake, L. Chen, B.C. Wang, and S.S. Taylor. 2010. Structure of D-AKAP2:PKA RI complex: insights into AKAP specificity and selectivity. *Structure*. 18:155–166. doi:10.1016/j.str.2009.12.012

Scott, J.D., M.B. Glaccum, M.J. Zoller, M.D. Uhler, D.M. Helfman, G.S. McKnight, and E.G. Krebs. 1987. The molecular cloning of a type II regulatory subunit of the cAMP-dependent protein kinase from rat skeletal muscle and mouse brain. *Proc. Natl. Acad. Sci. USA*. 84:5192–5196. doi:10.1073/pnas.84.15.5192

Steinberg, R.A., and D.A. Agard. 1981. Turnover of regulatory subunit of cyclic AMP-dependent protein kinase in S49 mouse lymphoma cells. Regulation by catalytic subunit and analogs of cyclic AMP. *J. Biol. Chem.* 256:10731–10734.

Takata, K., T. Matsuzaki, Y. Tajika, A. Ablimit, and T. Hasegawa. 2008. Localization and trafficking of aquaporin 2 in the kidney. *Histochem. Cell Biol.* 130:197–209. doi:10.1007/s00418-008-0457-0

Tanner, S., H. Shu, A. Frank, L.C. Wang, E. Zandi, M. Mumby, P.A. Pevzner, and V. Bafna. 2005. InsPecT: identification of posttranslationally modified peptides from tandem mass spectra. *Anal. Chem.* 77:4626–4639. doi:10.1021/ac050102d

Thiele, T.E., B. Willis, J. Stadler, J.G. Reynolds, I.L. Bernstein, and G.S. McKnight. 2000. High ethanol consumption and low sensitivity to ethanol-induced sedation in protein kinase A-mutant mice. *J. Neurosci.* 20:RC75.

Tortora, G., S. Pepe, C. Bianco, G. Baldassarre, A. Budillon, T. Clair, Y.S. Cho-Chung, A.R. Bianco, and F. Ciardiello. 1994a. The RI alpha subunit of protein kinase A controls serum dependency and entry into cell cycle of human mammary epithelial cells. *Oncogene*. 9:3233–3240.

Tortora, G., S. Pepe, C. Bianco, V. Damiano, A. Ruggiero, G. Baldassarre, C. Corbo, Y.S. Cho-Chung, A.R. Bianco, and F. Ciardiello. 1994b. Differential effects of protein kinase A sub-units on Chinese-hamster-ovary cell cycle and proliferation. *Int. J. Cancer*. 59:712–716. doi:10.1002/ijc.2910590521

Uhler, M.D., and G.S. McKnight. 1987. Expression of cDNAs for two isoforms of the catalytic subunit of cAMP-dependent protein kinase. *J. Biol. Chem.* 262:15202–15207.

van Niel, G., I. Porto-Carreiro, S. Simoes, and G. Raposo. 2006. Exosomes: a common pathway for a specialized function. *J. Biochem.* 140:13–21. doi:10.1093/jb/mvj128

Veugelers, M., D. Wilkes, K. Burton, D.A. McDermott, Y. Song, M.M. Goldstein, K. La Perle, C.J. Vaughan, A. O'Hagan, K.R. Bennett, et al. 2004. Comparative PRKAR1A genotype-phenotype analyses in humans with Carney complex and prkar1a haploinsufficient mice. *Proc. Natl. Acad. Sci. USA*. 101:14222–14227. doi:10.1073/pnas.0405535101

Wong, W., and J.D. Scott. 2004. AKAP signalling complexes: focal points in space and time. *Nat. Rev. Mol. Cell Biol.* 5:959–970. doi:10.1038/nrm1527

Yang, W.L., L. Iacono, W.M. Tang, and K.V. Chin. 1998. Novel function of the regulatory subunit of protein kinase A: regulation of cytochrome c oxidase activity and cytochrome c release. *Biochemistry*. 37:14175–14180. doi:10.1021/bi981402a

Yuan, H., A.A. Gerencser, G. Liot, S.A. Lipton, M. Ellisman, G.A. Perkins, and E. Bossy-Wetzel. 2007. Mitochondrial fission is an upstream and required event for bax foci formation in response to nitric oxide in cortical neurons. *Cell Death Differ.* 14:462–471. doi:10.1038/sj.cdd.4402046

Published April 18, 2011

Day et al., http://www.jcb.org/cgi/content/full/jcb.201010034/DC1

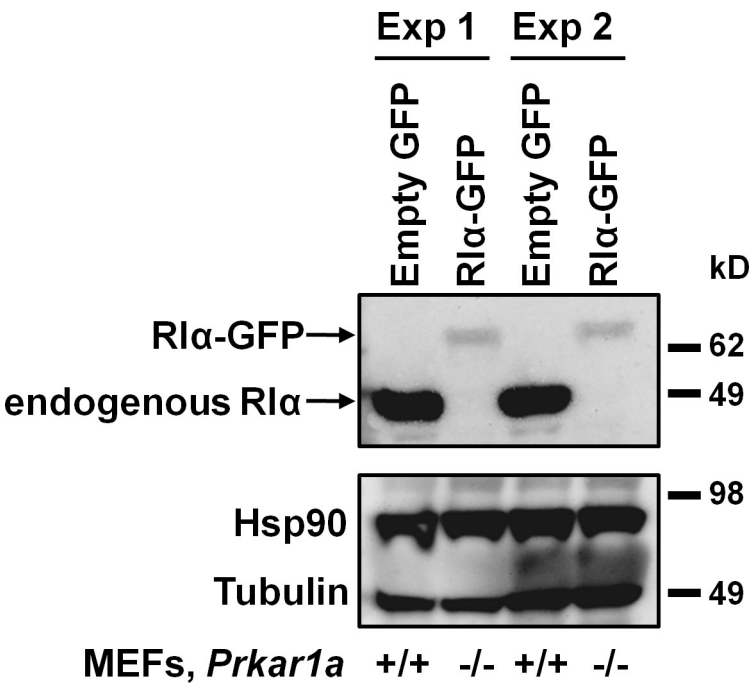

Figure S1. **RIα-GFP punctate pattern is not an artifact of overexpression.** *Prkar1a*$^{+/+}$ MEFs were transiently transfected with empty GFP as a control. *Prkar1a*$^{-/-}$ MEFs were transiently transfected with RIα-GFP, with a mean transfection efficiency of 15–30%. Two separate experiments (Exp) are shown. Samples from the whole-cell lysate were immunoblotted with antibodies against RIα, Hsp90, or tubulin. Lysates are 5 µg of total protein.

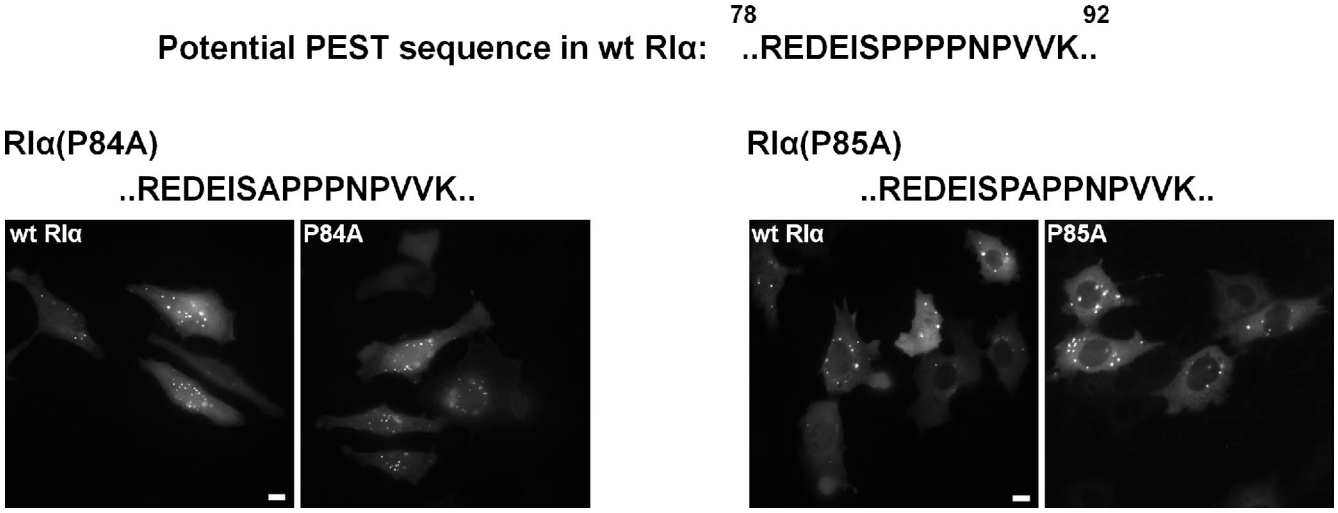

Figure S2. **Ubiquitination of RIα is not the signal for targeting to MVBs.** The putative PEST sequence identified in RIα (Bergold et al., 1992) was corroborated by a PEST sequence predictor, ePESTfind. Two single proline mutations that remove the PEST sequence, P84A and P85A, were expressed in *Prkar1a*$^{-/-}$ MEFs. wt, wild type. Bars, 20 µm.

Published April 18, 2011

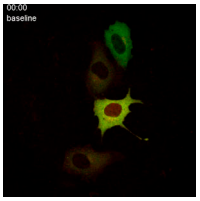

Video 1. **RIα puncta formation is reversible and independent of PKA activity.** Live-cell imaging of *Prkar1a*$^{-/-}$ MEFs transiently transfected with RIαGFP (green) and PKAc-mCherry (red). Events and times (in minutes) are labeled. Video speed is two frames/second. Cells went through three rounds of forskolin/IBMX treatments with four washes in between. Cells were kept at baseline for ∼8.5 min before the first round of forskolin/IBMX treatment. Then, forskolin/IBMX was left on cells for ∼18 min before the first set of washes. Cells were left without treatment for ∼9 min. Second treatment of forskolin/IBMX was left on cells for ∼13 min before the second set of washes. H89 was added to the cells for ∼9 min before addition of a third treatment of forskolin/IBMX. Cells were then left in forskolin/IBMX for the remainder of the video.

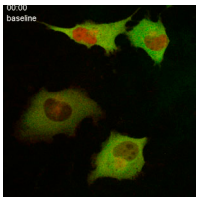

Video 2. **RIα puncta does not undergo rapid degradation.** Live-cell imaging of *Prkar1a*$^{-/-}$ MEFs transiently transfected with RIα-GFP (green) and PKAc-mCherry (red). Events and times (in minutes) are labeled. Video speed is two frames/second. Cells went through two rounds of forskolin/IBMX treatments with three washes in between. Cells were kept at baseline for ∼4 min before the first round of forskolin/IBMX treatment. Then, forskolin/IBMX was left on cells for ∼1.5 h before the washes. Cells were left without treatment for ∼45 min before the second round of forskolin/IBMX treatment. Cells were then left in forskolin/IBMX for the remainder of the video.

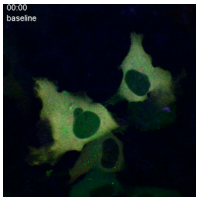

Video 3. **RIα puncta formation is not reversible in the presence of PKI.** Live-cell imaging of *Prkar1a*$^{-/-}$ MEFs transiently transfected with RIα-GFP (green), PKAc-mCherry (red), and PKI-CFP (blue). Events and times (in minutes) are labeled. Video speed is two frames/second. Cells went through one round of forskolin/IBMX treatment with four washes afterward. Cells were kept at baseline for ∼2.5 min before addition of forskolin/IBMX. Forskolin/IBMX was left on cells for ∼16 min before washes. Cells were left without treatment for the remainder of the video.

Published April 18, 2011

Table S1. **cAMP-binding proteins and their interacting partners identified from untransfected HEK 293 cells when using cAMP resin for purification**

Protein description	IPI	Number of hits	Unique peptides
PKA type I-α R-subunit	IPI00021831	64	19
PKA type II-α R-subunit	IPI00219774	104	31
PKA type II-β R-subunit	IPI00554752	6	4
AKAP9	IPI00019223	148	70
AKAP1	IPI00022585	9	5
Tubulin, β chain	IPI00011654	30	20
Tubulin, α-ubiquitous chain	IPI00387144	18	8
Tubulin, β-2c chain	IPI00007752	7	5
Vimentin	IPI00418471	35	18
Glyceraldehyde-3-phosphate dehydrogenase	IPI00219018	40	15
Phosphodiesterase 4D interacting protein	IPI00337544	22	9
Actin	IPI00848058	16	8
Histone H2B type 1-J	IPI00515061	11	7
Histone H2B	IPI00815755	3	2
Histone H2A.J	IPI00220855	5	2
Heterogeneous nuclear ribonucleoprotein K	IPI00216049	7	6
Heterogeneous nuclear ribonucleoprotein H1	IPI00479191	5	3
Heterogeneous nuclear ribonucleoprotein L	IPI00027834	2	2
Heterogeneous nuclear ribonucleoprotein M	IPI00171903	3	2
Heat shock 60-kD protein, mitochondrial	IPI00472102	8	5
Elongation factor 1–α1	IPI00396485	17	5
Pyruvate kinase isozymes M1/M2	IPI00783061	15	5
Macrophage migration inhibitory factor	IPI00293276	9	5
60S ribosomal protein L13	IPI00465361	5	4
60S ribosomal protein L6	IPI00790342	5	3
60S ribosomal protein L24	IPI00793696	2	2
60S ribosomal protein L8	IPI00012772	3	2
T-complex protein 1 subunit β	IPI00290770	4	4
T-complex protein 1 subunit θ	IPI00784090	4	3
T-complex protein 1 subunit ζ	IPI00027626	3	3
T-complex protein 1 subunit δ	IPI00302927	2	2

IPI, International Protein Index.

Published April 18, 2011

Table S2. **cAMP-binding proteins and their interacting partners identified from HEK 293 cells stably expressing TAP-tagged wild-type RIα when using cAMP resin for purification**

Protein description	IPI	Number of hits	Unique peptides
PKA type I-α R-subunit	IPI00021831	57	19
PKA type II-α R-subunit	IPI00219774	15	12
PKA type II-β R-subunit	IPI00554752	9	6
AKAP11	IPI00007411	9	8
AKAP9	IPI00220628	5	4
AKAP5	IPI00307794	2	2
Myosin-9	IPI00019502	586	240
Isoform 3 of myosin-10	IPI00790503	171	98
Isoform 1 of myosin-8A	IPI00017030	37	24
Myosin-6	IPI00844172	25	20
Myosin-1C	IPI00743335	24	14
Isoform 2 of myosin-14	IPI00607818	12	10
Isoform 2 of myosin-1B	IPI00414980	16	11
Isoform 1 of myosin-1D	IPI00329719	7	6
Isoform 1 of myosin-5A	IPI00000807	2	2
Actin, β	IPI00848058	365	106
Actin, α cardiac muscle 1	IPI00023006	53	16
Actin, cytoplasmic 1	IPI00021439	11	2
Drebrin	IPI00003406	50	27
Isoform 3 of tropomyosin-1 α chain	IPI00216135	39	25
Isoform 1 of tropomyosin-4 α chain	IPI00010779	13	10
Isoform 2 of tropomyosin-3 α chain	IPI00218319	13	7
Isoform β of LIM domain and actin-binding protein 1	IPI00008918	38	23
Vimentin	IPI00418471	34	23
Isoform 1 of myosin phosphatase Rho-interacting protein	IPI00305344	26	22
Cytospin-A	IPI00178072	27	18
Tubulin, β	IPI00645452	10	10
Tubulin, α-ubiquitous chain	IPI00387144	7	6
Glyceraldehyde-3-phosphate dehydrogenase	IPI00219018	29	15
Isoform 1 of ankycorbin	IPI00759532	17	15
Myosin regulatory light chain	IPI00033494	52	14
Isoform nonmuscle of myosin light polypeptide 6	IPI00335168	34	13
Myosin light polypeptide 6B	IPI00027255	4	3
Myosin LC3, skeletal muscle isoform	IPI00220332	12	2
Spectrin, α	IPI00744706	22	13
Spectrin, β, nonerythrocytic 1 isoform 1 variant	IPI00794135	10	8
filamin A, α	IPI00302592	13	12
Poly [ADP-ribose] polymerase 1	IPI00449049	14	11
Elongation factor 1–α 1	IPI00847435	18	11
Elongation factor 2	IPI00186290	2	2
60S ribosomal protein L4	IPI00003918	17	9
60S ribosomal protein L27a	IPI00456758	5	3
60S ribosomal protein L13	IPI00465361	3	3
60S ribosomal protein L3	IPI00550021	4	3
60S ribosomal protein L19	IPI00025329	2	2
60S ribosomal protein L6	IPI00329389	2	2
60S ribosomal protein L35	IPI00412607	2	2
Casein kinase II	IPI00016613	7	7
Casein kinase II subunit β	IPI00010865	2	2
Casein kinase II subunit α	IPI00020602	3	2
Isoform A2 of heterogeneous nuclear ribonucleoproteins A2/B1	IPI00414696	8	7
Heterogeneous nuclear ribonucleoprotein U isoform a	IPI00644079	7	6
Isoform 3 of heterogeneous nuclear ribonucleoprotein K	IPI00807545	5	3
Isoform 1 of heterogeneous nuclear ribonucleoprotein M	IPI00171903	2	2
Isoform 1 of heterogeneous nuclear ribonucleoprotein A3	IPI00419373	3	2
Similar to heterogeneous nuclear ribonucleoprotein A1	IPI00738822	2	2
Heterogeneous nuclear ribonucleoprotein L isoform b	IPI00465225	2	2

Published April 18, 2011

Table S2. **cAMP-binding proteins and their interacting partners identified from HEK 293 cells stably expressing TAP-tagged wild-type RIα when using cAMP resin for purification** *(Continued)*

Protein description	IPI	Number of hits	Unique peptides
Histone H2A type 1-J	IPI00552873	16	7
Histone H4	IPI00453473	11	6
Histone H2B type 1-J	IPI00515061	13	6
Histone H1.4	IPI00217467	4	3
Histone H1.2	IPI00217465	2	2
Histone H2A.X	IPI00219037	2	2
40S ribosomal protein S6	IPI00021840	7	4
40S ribosomal protein S8	IPI00216587	3	3
40S ribosomal protein S13	IPI00221089	5	3
40S ribosomal protein S14	IPI00026271	3	2

IPI, International Protein Index.

Table S3. **RIα holoenzymes and their interacting proteins identified from HEK 293 cells stably expressing TAP-tagged wild-type RIα when using streptavidin resin followed by calmodulin resin for purification**

Protein description	IPI	Number of hits	Unique peptides
PKA type I-α R-subunit	IPI00021831	434	29
PKA, α-catalytic subunit	IPI00217960	2	2
PKA, α-catalytic subunit	IPI00396630	6	3
AKAP11	IPI00007411	13	9
Myosin-9	IPI00019502	29	19
Actin, cytoplasmic 1	IPI00021439	10	7
Actin, β	IPI00848058	10	7
Tubulin, α-ubiquitous chain	IPI00387144	5	3
Tubulin, β chain	IPI00011654	4	2
Histone H2A type 3	IPI00031562	5	2
Isoform 1 of myosin-1B	IPI00376344	3	2
Isoform short of heterogeneous nuclear ribonucleoprotein U	IPI00479217	3	2

IPI, International Protein Index.

Published April 18, 2011

Table S4. **RIα-binding proteins identified from HEK 293 cells stably expressing TAP-tagged wild-type RIα when using streptavidin resin followed by cAMP resin for purification (more than three unique peptides)**

Protein description	IPI	Number of hits	Unique peptides
PKA type I-α R-subunit	IPI00021831	721	63
PKA type I-β R-subunit	IPI00787996	21	14
AKAP11	IPI00007411	113	59
Myosin-9	IPI00019502	98	81
Actin, cytoplasmic 1	IPI00021439	59	41
Actin, α cardiac muscle 1	IPI00023006	6	4
Acetyl-CoA carboxylase 1	IPI00011569	17	17
Isoform 2 of Acetyl-CoA carboxylase 1	IPI00847501	8	8
Methylcrotonoyl-CoA carboxylase subunit α, mitochondrial precursor	IPI00024580	9	7
Drebrin 1	IPI00794221	7	6
Heat shock 70-kD protein 8 isoform 2 variant (fragment)	IPI00795040	6	6
Myosin-1B	IPI00795618	6	6
HSPA5 protein	IPI00003362	7	4
EF-hand domain-containing protein 2	IPI00060181	6	4
Tropomyosin 3 isoform 5	IPI00477649	4	4
ACTA2 protein (fragment)	IPI00816229	5	3
Stomatin-like protein 2	IPI00334190	4	3
40S ribosomal protein S3	IPI00011253	3	3
Isoform 1 of myosin-1D	IPI00329719	3	3
Heterogeneous nuclear ribonucleoprotein L isoform b	IPI00465225	3	3

IPI, International Protein Index.

Reference

Bergold, P.J., S.A. Beushausen, T.C. Sacktor, S. Cheley, H. Bayley, and J.H. Schwartz. 1992. A regulatory subunit of the cAMP-dependent protein kinase down-regulated in aplysia sensory neurons during long-term sensitization. *Neuron*. 8:387–397. doi:10.1016/0896-6273(92)90304-V